A 125-ka record of northern South American precipitation and the role of high-to-low latitude teleconnections

A. Zhuravleva[1,2,3], M. Hüls[4], R. Tiedemann[5], and H. A. Bauch[6]

[1]Academy of Sciences, Humanities and Literature, Geschwister-Scholl-Str. 2, 55131 Mainz, Germany

[2]GEOMAR Helmholtz Centre for Ocean Research Kiel, Wischhofstr. 1-3, 24148 Kiel, Germany

[3]Department of Oceanography, Dalhousie University, 1355 Oxford Street, Halifax, NS B3H4R2, Canada

[4]Leibniz-Laboratory for Radiometric Dating and Isotope Research, Kiel University, Max-Eyth-Straße 11-13, 24118 Kiel, Germany

[5]Alfred Wegener Institute, Helmholtz Centre for Polar and Marine Research, Am Alten Hafen 26, Bremerhaven 27568, Germany

[6]Alfred Wegener Institute, Helmholtz Centre for Polar and Marine Research c/o GEOMAR Helmholtz Centre for Ocean Research Kiel, Wischhofstr. 1-3, 24148 Kiel, Germany

Corresponding author: Anastasia Zhuravleva (anastasia.zhuravleva@dal.ca)

Postal address: Anastasia Zhuravleva, Department of Oceanography, Dalhousie University, 1355 Oxford Street, Halifax, NS, B3H 4R2, Canada

Highlights:

- Lowered Orinoco River sediment discharge during stadials due to more arid conditions in northern South America
- Reduced supply of Amazonian sediments to the SE Caribbean during stadials due to reorganization of ocean surface currents
- SE Caribbean Sea warmed during cold Greenland stadials due to AMOC changes and the bipolar seesaw

Keywords:

South America, ITCZ, Orinoco River, Amazon River, Climate teleconnections, Sedimentology-marine cores

Abstract

The occurrence of rapid last glacial temperature shifts in both Greenland ice and subpolar marine sediment cores, so-called Dansgaard-Oeschger (D-O) cycles, is evidence of a tight regional climate connectivity in these northern latitudes. By contrast, processes behind high-to-low-latitude teleconnections during the D-O cycles are less well understood, due to imprecisions in cross-dating marine and ice core records and a general lack of solid multi-proxy records from the tropical region. Here we aim to study the response of the tropical ocean-atmosphere system to D-O variability by using a sediment core from the southern Caribbean Sea, located under the direct influence of the Intertropical Convergence Zone (ITCZ) and the Atlantic meridional overturning circulation (AMOC). During D-O cycles, abrupt shifts in the deposition of fine-grained terrigenous material sourced from the Orinoco and Amazon Rivers are recognized. These sedimentary changes were associated with fluctuations in both the ITCZ location and the AMOC strength through their respective influence on the hydroclimate of northern South America and strength of ocean currents delivering fluvial material to the study site. Stable oxygen isotope data further suggest increase in the upper ocean temperatures in the southeastern Caribbean Sea during stadial events. As these warming trends correlate with Antarctic temperatures, they seem to contain imprints of the bipolar seesaw and AMOC variability, demonstrating that our core location was influenced by processes prevalent in both hemispheres.

1 Introduction

Abrupt shifts in Greenland and North Atlantic temperatures – termed Dansgaard-Oeschger (D-O) cycles - characterized the last glacial period (MIS 2-4). Millennial-scale climate oscillations were also pronounced during the relatively warm MIS 5a-5d, probably due to fluctuations in the range of an average ice volume. In the low-latidudes, the D-O cycles were associated with abrupt changes in precipitation, well-expressed in speleothems and lacustrine records from South America and neotropics (Hodell et al., 2008; Cruz et al., 2009; Escobar et al., 2012; Kanner et al., 2012; Mosblech et al., 2012; Cheng et al., 2013; Baker & Fritz, 2015; Zhang et al., 2017; Caballero et al., 2019; Corrick et al., 2020; Warken et al., 2020). Likewise, marine sedimentary records reveal significant climate variability associated with D-O events. In particular, proxies for river discharge from the Cariaco Basin off northern Venezuela demonstrate strongly reduced run-off during cold stadials in Greenland (Peterson et al., 2000; Haug et al., 2001; Deplazes et al., 2013; Gibson & Peterson, 2014). Coevally, enhanced humidity characterized the southern hemishpere, as evidenced from both speleothem records from western Amazonia, tropical Andes, and Brazil and marine sedimentary records obtained off the northeastern South American continental margin (Arz et al., 1998; Jaeschke et al., 2007; Wang et al., 2007; Mosblech et al., 2012; Govin et al., 2014; Nace et al., 2014; Zhang et al., 2015b, 2017; Mulitza et a. 2017; Venancio et al., 2018; Stríkis et al., 2018; Piacsek et al., 2021). Thus, paleoclimate records provide ample evidence for a tight and fast linkage between high-latitudinal North Atlantic climate and South American precipitation on centennial to millennial timescales.

The mechanism responsible for this high-to-low latitude coupling involves meridional shifts in the mean position of the Intertropical Convergence Zone, the ITCZ (Wang et al., 2007).

The ITCZ is defined as a region where southeastern and northeastern Atlantic trade winds converge and is associated with heavy precipitation (Poveda et al., 2006; Martinez et al., 2019). Observations suggest that the mean latitude of the ITCZ is controlled by the sea surface temperature (SST) gradient between the relatively warm North Atlantic and the relatively cool South Atlantic (Chiang et al., 2002). In models, ITCZ position was shown to be sensitive to climate change in the high northern latitudes. In particular, it was suggested that North Atlantic cooling (e.g., a result of sea ice expansion) can propagate towards the equator, influence the interhemispheric SST gradient and thereby cause a southward ITCZ shift (Chiang et al., 2003; Chiang & Bitz, 2005; Chiang & Friedmann, 2012). On millennial timescales, ITCZ movements have been linked to changes in the interhemispheric heat redistribution via the Atlantic meridional overturning circulation (AMOC) through the global (atmosphere and ocean) energy budget; thus AMOC weakening and associated reductions in northward oceanic heat transport would be accompanied by a stronger northward cross-equatorial atmospheric energy transport that would shift the mean postion of the ITCZ southwards (Dahl et al., 2005; Broccoli et al., 2006; Schneider et al., 2014; Mulitza et al., 2017).

Despite intense research, there is no consensus with regard to the sequence of events and forcing mechanisms that triggered the D-O cycles (for reviews see Li & Born, 2019; Menviel et al., 2020). Proxy data and climate models indicate that changes in the AMOC strength were involved in D-O variability (Burkel et al., 2015; Henry et al., 2016; Gottschalk et al., 2018; Boers et al., 2018). However, it remains unclear whether variations in the AMOC strength were an independent trigger of D-O cycles or the AMOC varied in response to the high northern latitudes changes (Lynch-Stieglitz, 2017). In addition, while evidence for the AMOC instabilities associated with the D-O cycles during the last glacial period is ample (Burckel et al., 2015; Gottschalk et al.,

2015; Zhang et al., 2015a; Henry et al., 2016), only limited and contradictory proxy data exist for the generally warmer MIS 5 with climatic settings more similar to the current Holocene interglacial (Thornalley et al., 2013; Böhm et al., 2015; Lynch-Stieglitz, 2017).

Knowledge of climatic processes that were involved in the D-O cycles can be improved through use of sedimentary archives from the southern Caribbean Sea: Because of their location at the crossroad of ITCZ influence and AMOC-related upper ocean flow from the southern hemisphere, regional multi-proxy marine records potentially bear information about the coupled response of the tropical ocean-atmosphere system to abrupt climate change in the high northern latitudes. Earlier studies in the Caribbean Basin, mostly confined to the last (de)glacial interval (MIS 1-4), reveal abrupt variations in terrigenous inputs, associated with ITCZ shifts, and more gradual changes in SSTs, linked with the bipolar seesaw mechanism (Rühlemann et al., 1999; Hüls & Zahn, 2000; Deplazes et al., 2013; Bahr et al., 2018). Nevertheless, detailed and long multi-proxy climate records that illustrate reorganizations of the tropical ocean-atmosphere system and its coupling with polar climate fluctuations are very sparse (but see e.g., Bahr et al., 2018).

To close this gap, we used a sediment core from the Tobago Basin (southeastern Caribbean Sea) and generated a continuous high-resolution record of sedimentary changes (using Ti/Ca and Zr/Rb) that were presumably linked with fluctuations in regional rainfall amounts. These results were then compared with proxy data for upper ocean properties (0-50 m water depths) using planktic $\delta^{18}O$ values from the same sediment core. We suggest that northern and southern high latitudinal processes influenced the tropical ocean-atmosphere system through their impact on the ITCZ location and ocean circulation during D-O climate cycles. This study therefore provides

123 important results to climate modelers and paleoclimatologists aiming to understand abrupt climate
124 change, high-latitude forcing of tropical (hydro)climate, as well as tropical ocean-atmosphere
125 feedback mechanisms.
126
127 **2 Regional setting**
128 *2.1 Hydroclimate*
129 Rainfall in the northern South America is controlled by the South American Monsoon
130 System (SAMS), which is driven by land-sea thermal contrasts (Cook, 2009). SAMS influences
131 the Amazon Basin between October and April, while during boreal summer-autumn the rainfall
132 shifts to the north of the equator (Fig. 1B; Poveda et al., 2006; Silva & Kousky 2012; Martinez
133 et al., 2019). Seasonal migration of the maritime ITCZ and its imbedded precipitation band follow
134 the region of warmest SST and directly influence the hydroclimate of the northeastern coastal
135 South America (Baker & Fritz, 2015). In addition, through its influence on the moisture influx to
136 the continent, the ITCZ dynamics is indirectly tied with the intensity of the SAMS (Vuille et al.,
137 2012). For instance, strengthened northeastern trade winds at times of a sourtherly displaced ITCZ
138 bring more moisture towards the Amazon Basin thereby promoting intensified convective activity
139 in that region (Fig. 1B; Martinez et al., 2019).
140

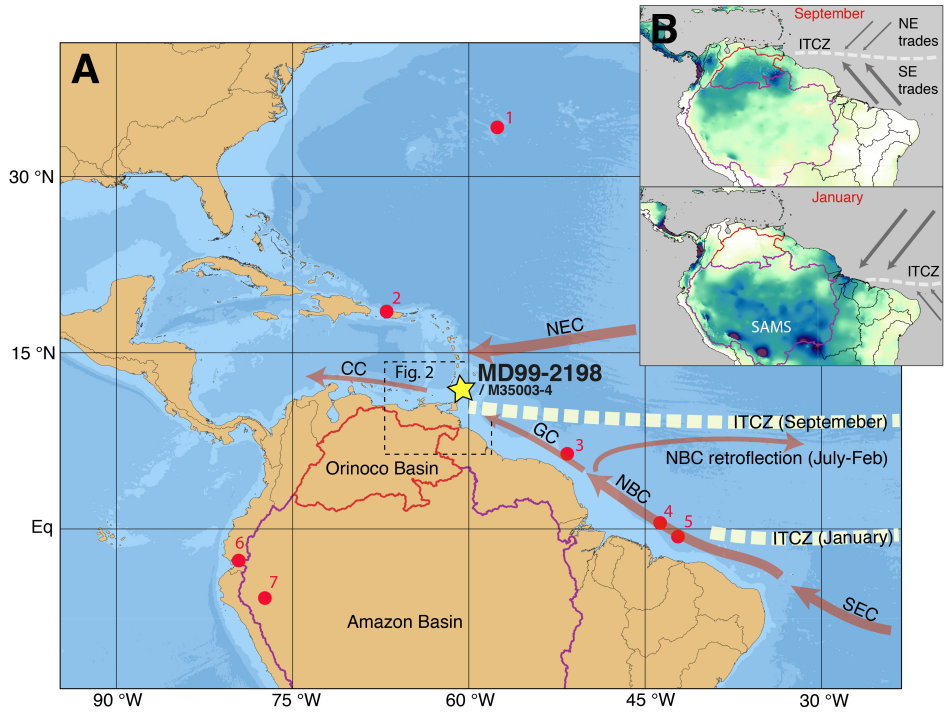

Figure 1. (A) Location of cores MD99-2198 and M35003-4 together with main hydrographic and atmospheric features in the western tropical Atlantic. Red dots show other relevant climatological sites discussed in the text: 1 – ODP Site 1063 (Böhm et al., 2015), 2 - speleothem from Larga Cave, Puerto-Rico (Warken et al., 2020), 3 – core GeoB16224-1 (Crivellari et al., 2019), 4 – core CDH-86 (Nace et al., 2014), 5 - core GL-1248 (Venancio et al., 2018), 6 – speleothem from Santiago Cave, Ecuador (Mosblech et al., 2012), and 7 - speleothem from Cueva del Diamante Cave, Peru (Cheng et al., 2013). Other relevant locations and a close-up of the study area (dashed square) are shown in Fig. 2. **(B)** Monthly precipitation maps of northern South America together with the location of the marine ITCZ (white dashed line) and trade winds system during boreal summer (upper panel) and boreal winter (lower panel). Maps are created using QGIS 3.10 (QGIS Development Team, 2020; http://qgis.osgeo.org). Bathymetry is from ETOPO11 Arc-Minute Relief Model (Amante & Eakins, 2009). River basins are from HydroATLAS version 1.0 (Lehner et al., 2019), total monthly precipitation for years 2010-2018 is from CRU-TS-4.03 (Harris

et al., 2014) dataset, downscaled with WorldClim 2.1 (Fick & Hijmans, 2017). CC – Caribbean Current; GC-Guyana Current; ITCZ – Intertropical Convergence Zone; NBC - North Brazil Current; NEC - North Equatorial Current, SAMS - South American Monsoon System; SEC – South Equatorial Current.

2.2 Oceanographic setting

While water masses from the northern and southern hemispheres converge in the eastern Caribbean Sea, the surface hydrography is defined by the North Equatorial Current (NEC) and a continuation of the North Brazil Current (NBC), the Guyana Current (Fig. 1; Johns et al., 1998; Schott et al., 1998). The NEC is driven by the northeastern trade winds and transports waters into the Caribbean Basin mainly north of 15 °N (Johns et al., 2002). The NBC, a northward flowing western boundary current, is forced predominantly by the AMOC, but also by the wind curl; it transports waters from the South Atlantic in the upper 150-300 m (Johns et al., 1998; Stramma & Schott, 1999; Johns et al., 2002; Zhang et al., 2011). Annual transport through the Grenada passage strongly varies seasonally in response to ITCZ migration and associated changes in wind strength. While maximum transport occurs during boreal spring-summer, inflows into the southern Caribbean are weakened from about July to February; this is a result of the NBC retroflection (near 6 °N) caused by development of a cyclonic circulation cell associated with a northern location of the ITCZ (Johns et al., 2002).

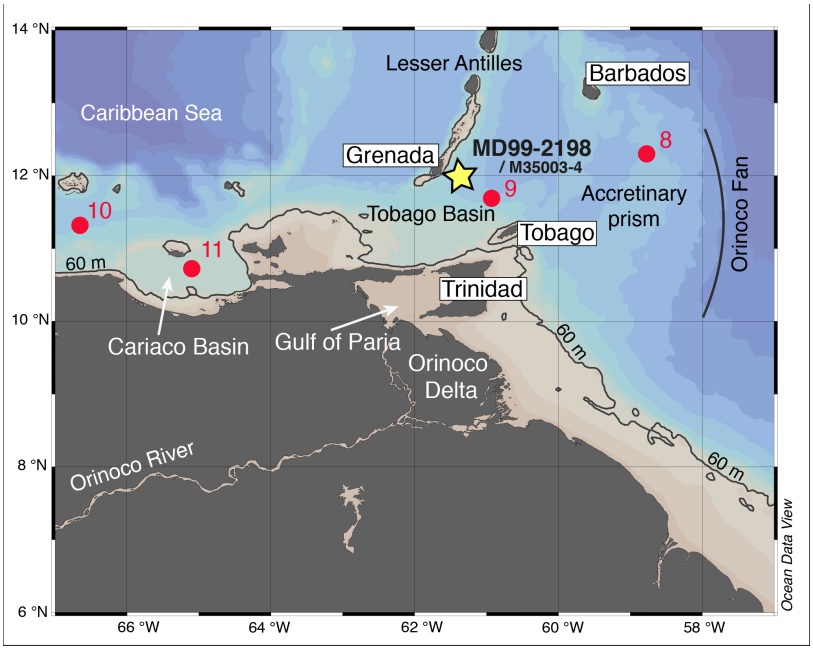

Figure 2. A close-up of the study area. Location of cores MD99-2198 and M35003-4 together with other relevant sediment cores discussed in the text (red dots): 8 – GeoB3938-1 (Govin et al., 2014), 9 - M78/1-235-110 (Bahr et al., 2018), 10 - core VM12-107 (Parker et al., 2015), 11 - MD03-2622 (Gibson & Peterson, 2014). Also shown is the 60-m isobath. Map is created using Ocean Data View (Schlitzer, 2017).

2.3 Sedimentation and fluvial inputs

Sediments in the Tobago Basin are predominantly pelagic in origin (foraminifera and coccoliths), but with significant terrigenous contributions from the nearby volcanic island of Grenada and from the Orinoco and Amazon Rivers (Fig. 2; Reid et al., 1996; Picard et al., 2006). According to estimations by Reid et al. (1996), volcanic silt and clay constitute about 50 % of sediments in the Tobago Trough just to the north from the Tobago Basin, whereas South American rivers contribute 20 % of clay-sized sediments (Fig. 9 in Reid et al., 1996). Because the Orinoco River transports ~7-8 times less material than the Amazon River, the Amazon-derived sediments

189 comprise about 50 % of material deposited along the Orinoco coast (Eisma et al., 1978; Meade,
190 1994; Warne et al., 2002). Almost the entire sediment load from the Amazon River is sourced from
191 the Andean mountains (Filizola et al., 2011; Govin et al., 2014; Rousseau et al., 2019; Armijos et
192 al., 2020). Likewise, about 90-95 % of the Orinoco's solid load is derived from left-bank tributaries
193 which drain the northern part of the Andean cordillera and Llanos, a wide area of alluvial plains
194 east of the Andes (Meade, 1994; Edmond et al., 1995; Mora et al., 2020).
195
196 The discharge from the Amazon Basin is linked to the SAMS, characterized by an
197 increased moisture influx to the continent at times of intensified northeastern trades and
198 strengthened land-sea thermal gradients during the boreal winter (Fig. 1B; Cook, 2009; Silva &
199 Kousky, 2012; Vuille et al., 2012; Baker & Fritz, 2015). Maximum precipitation occurs over the
200 Amazon Basin in January-February (Armijos et al., 2020). The highest Orinoco River discharge
201 from the Andean streams occurs during boreal summer, when the ITCZ is shifted northwards,
202 whereas 30-40 % of the river channel bottom may be aerially exposed during dry season in winter
203 (Warne et al., 2002). In particular, Colombian Andes that provide about 70 % of the total annual
204 Orinoco sediment load generally experience wet season between April and November with
205 somewhat less rain in June-August as a result of double passage of the ITCZ (Fig. 2 in Poveda et
206 al., 2006).
207
208 Amazon River sediments are transported along the shoreline of the South American
209 continent by the NBC and the Guyana Current (Fig. 1). While between July and December the
210 sediments become entrained into the NBC retroflection and advected eastwards into the open
211 ocean, during the spring-summer season (i.e., during peak of sediment discharge; Martinez et al.,

2009; Armijos et al., 2020), the Amazon-derived sediments are transported northwards by the oceanic currents (Muller-Karger et al., 1988). Most of these sediments are deposited along the Guyana and Suriname margins, however, some reach the Orinoco Delta where they become mixed with the Orinoco River sediments (Warne et al., 2002). The Amazon and Orinoco-derived sediments are then predominantly transported through the Gulf of Paria and into the central Caribbean Basin (Fig. 2; Milliman et al., 1982; Bowles & Fleischer, 1985; Meade, 1994). Only a small portion of fluvial sediments is transported along the eastern margin of Trinidad within the deflected branch of the Guyana Current and reaches the Tobago Basin (Meade, 2007).

3 Material and Methods

3.1 Material

Giant piston core MD99-2198 (12° 05′ N, 61° 14′ W, 1330 m water depth) was collected in 1999 during IMAGES campaign of R/V Marion Dufresne (Figs. 1-2; Labeyrie, 1999). The core is from the western flank of the Tobago Basin (southeastern Caribbean Sea), just to the east off the volcanic island of Grenada and from the same site as core M35003-4 (12° 05′ N, 61° 15′ W, 1299 m water depth; Hemleben et al., 1998).

3.2 Preliminary data treatment

Following Griffiths et al. (2013) we modified the core depth scale in core MD99-2198 by excluding two intervals (10.06-10.24 m and 13.78-14.30 m), representing sections where the core was pulled apart by the force of the piston during coring. This process is firmly concluded on the basis of large increases in porosity (Labeyrie & Zahn, 2005a) and from comparison with the magnetic susceptibility record from core MD99-2199 (Figs. S1-S2). This latter core was retrieved

just 3 km southeastward from MD99-2198 and yields very similar magnetic susceptibility values and patterns that can be easily correlated to our core (Labeyrie & Zahn, 2005a, b). In addition, we filled the gap in magnetic susceptibility values in core MD99-2198 for core depths 8.22-9.06 m, by using the magnetic susceptibility profile from core MD99-2199 (Fig. S3).

3.3 X-ray fluorescence (XRF) scanning

XRF analysis was performed using the Aavatech XRF Core Scanner at Christian-Albrecht University Kiel in two runs (10 kv, 750 μA, 10 seconds and 30 kv, 2000 μA, 20 seconds). The surface of the sediment was smoothed and covered with a 4 μm-thick ULTRALENE SPEXCerti Prep film to prevent contamination of the measurement unit and desiccation of the sediment (Richter et al., 2006; Tjallingii et al., 2007). Elemental intensities were measured every 10 mm between 0-18.83 m and 5 mm for the core section between 18.84-22 m (here and below the revised depth is used, see 3.2).

To reduce the measurement artefacts (i.e., shifts in elemental intensities between different core sections), we have divided the raw counts of each element by the sum of all processed elements for a given run, excluding rhodium intensity for a 10-kv run, because this element is biased by the signal generation (Bahr et al., 2014). Afterwards, we normalized our XRF data, by bringing the total sum of elemental data to 100 % (Lyle et al., 2012). To account for a statistically more robust representation of elemental ratios, we use log-ratios following the suggestion of Weltje & Tjallingii (2008). Outliers have been removed for XRF data using QAnalyseries, based on standard deviation limits of the data (Kotov & Pälike, 2019). Data smoothing (3 times 3-point-moving average) was made using the program PAST 4.02 (Hammer et al., 2001).

258

259 *3.4 Stable oxygen isotopes ($\delta^{18}O$)*

260 Samples were taken each 10-20 cm throughout the upper 18.5 m of the core and at 10 cm
261 resolution between 18.5-22 m. $\delta^{18}O$ values were measured on 5 specimens (>250 μm size fraction)
262 of planktic foraminifera *Globigerinoides sacculifer*, using a CARBO KIEL automated carbonate
263 preparation device and a FINNIGAN MAT 252 mass spectrometer. Reproducibility for the
264 analyses was better than 0.066 ‰ (n=80). $\delta^{18}O$ values are referred to the Vienna Pee Dee
265 Belemnite (VPDB) through calibration with NBS-19.

266

267 *3.5 $CaCO_3$*

268 Samples were taken at 10-20 cm throughout the upper ~11 m of the core and at 5 cm
269 between 11-22 m. Total carbon (TC) concentrations were determined by combustion on a LECO
270 analyser with reproducibility better than ±1 % of the measured value (see Vink et al., 2001). For
271 total organic carbon (TOC), inorganic carbon was measured from decalcified samples and then it
272 was subtracted from the TC in the sample. The carbonate content was calculated as $CaCO_3 = 8.33x$
273 (TC-TOC).

274

275 **4 Age model**

276 The age model for core MD99-2198 is based on (a) radiocarbon dates, (b) core-to-core
277 correlations, and (c) alignment to the Greenland $\delta^{18}O$ record (Fig. 3; Table S1):

278

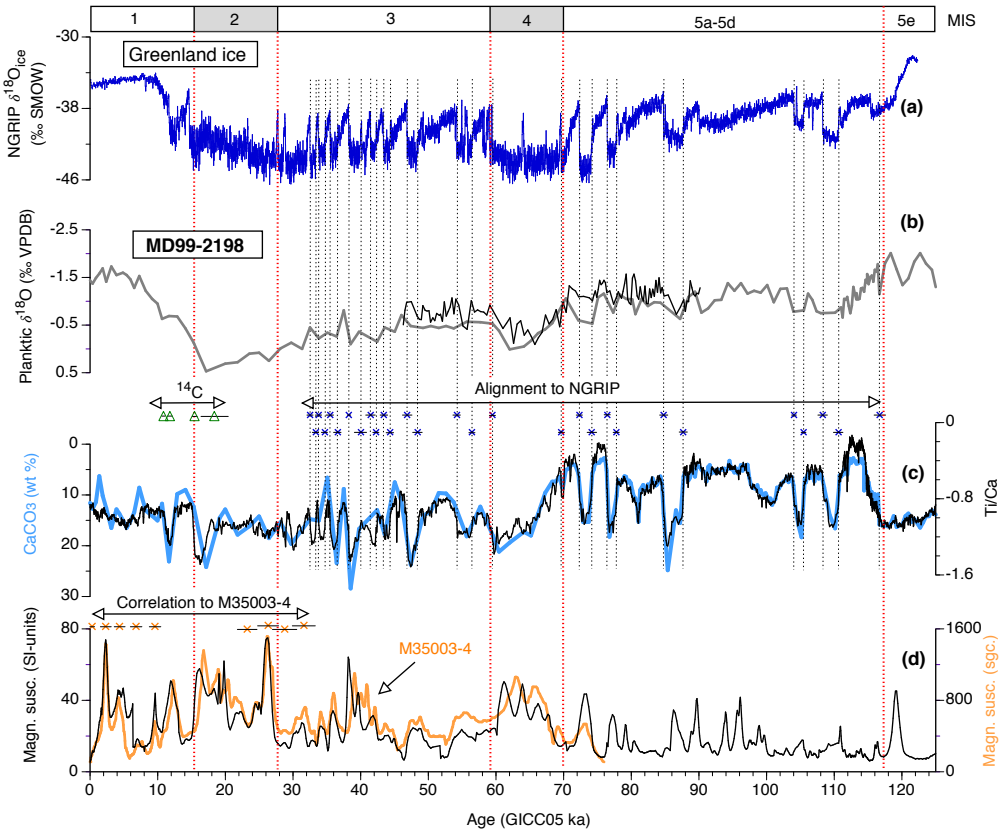

Figure 3. Chronology of core MD99-2198. **(a)** Greenland ice $\delta^{18}O$ record (NGRIP Members, 2004), **(b)** $\delta^{18}O$ values in *G. sacculifer* (grey) and more densely-sampled $\delta^{18}O$ values in *G. ruber* (white) (black) between 45-90 ka in MD99-2198 (this study and Griffiths et al. (2013), respectively), **(c)** log-ratios of Ti/Ca (black), which mirror $CaCO_3$ content (blue) in MD99-2198, **(c)** magnetic susceptibility records of MD99-2198 (black; Labeyrie & Zahn, 2005a) and M35003-4 (orange; Frank et al., 2017). Age model in core MD99-2198 is based on 4 radiocarbon dates (green triangles; Pahnke et al., 2008), alignment of Ti/Ca values to Greenland ice core $\delta^{18}O$ record (blue crosses) and correlations to core M35003-4 (orange crosses). Also shown are age uncertainties (95 % confidence intervals) for both radiocarbon dates and tie points (Table S1). Core-to-core correlations and alignments to the ice core were made using the AnalySeries program (Paillard et al., 1996). MIS – marine isotope stage.

(a) Four radiocarbon dates available from Pahnke et al. (2008) were recalibrated in BACON (Fig. S4; Blaauw & Christen, 2011) using IntCal13 calibration curve with a reservoir age 467 ±119 (Reimer et al., 2013; Waelbroeck et al., 2019). We did not use regional correction (ΔR), which is sensitive to properties of sea surface water masses, because of possible rapid changes in ΔR at our site during glacial times in response to proposed changing surface currents (Vink et al., 2001). We note that in the present-day Caribbean Sea ΔR values in the northern regions and under the influence of the NEC are somewhat higher (36 ± 26 yr; Kilbourne et al., 2007) when compared to the average Caribbean values within the influence of the southern-sourced waters of the NBC (-32 ± 25 yr; Wagner et al., 2009). We further note that possible changes in global and local radiocarbon reservoir ages in response to ocean circulation changes as well as uncertainties associated with conversion of radiocarbon ages into calendar ages can hinder accurate dating of the sediment core and result in large age uncertainties, especially during the last deglaciation (Fig. 3).

(b) The upper portion of core MD99-2198 (covering Holocene and MIS 2; stratigraphy is supported by $\delta^{18}O$ values in *G. sacculifer*, Fig. 3b) was correlated to the radiocarbon-dated core M35003-4, using magnetic susceptibility records (Fig. 3d; Labeyrie & Zahn, 2005a; Frank et al., 2017). Core M35003-4 was taken from the same location as MD99-2198 and its chronology was revisited and improved in the supplementary (Text S1).

(c) Because radiocarbon-dated cores from the Tobago Basin show a good correspondence between sediment lightness/$CaCO_3$ and Greenland climate (Hüls & Zahn, 2000; Bahr et al., 2018; Nürnberg et al., 2021), we aligned our high-resolution Ti/Ca record, which mirrors $CaCO_3$ content

(Fig. 3c), to the North Greenland Ice Core Project (NGRIP) $\delta^{18}O$ record on the GICC05 timescale between 32 and 110 ka (Fig. 3a; NGRIP Members, 2004; Rasmussen et al., 2014). Pronounced increases/reductions in Ti/Ca values were aligned with corresponding transitions into interstadial/stadial conditions over Greenland. We note that $CaCO_3$ peaks associated with Greenland stadials cannot be linked to carbonate-rich turbidites because of much higher $CaCO_3$ content in these episodic layers (Reid et al., 1996). Following recommendations of the INTIMATE protocol (Rasmussen et al., 2014), we further note that the term Heinrich Stadial will be used to refer to a stadial containing a particular Heinrich Event with according numbering. The so-called Heinrich Events, found in sediments from the North Atlantic during several longer stadials, are massive layers of ice-rafted debris accumulated as a result of iceberg surges (Bond et al., 1993; Marcott et al., 2011). Finally, we framed the MIS 5e "plateau", by correlating our $\delta^{18}O$ values in *G. sacculifer* to North Atlantic records (Govin et al., 2015).

The age uncertainties associated with the tie points depend on our ability to identify climatic events (e.g., D-O cycles) in our proxy data and to match them with the ice core and reference sediment core M35003-4. Because stadial/interstadial transitions in our Ti/Ca record are pronounced and occur rapidly (normally within 2-4 cm) and because of high sedimentation rates at our site (between 10 and 40 cm/kyr; Fig. 4e), the age uncertainties associated with the D-O cycles are estimated to be rather low and fall between 250-700 years (Table S1). Additional age uncertainties may emerge as a result of bioturbation bias, particularly during episodes of low accumulation rates like the time interval corresponding to Heinrich Stadial 1. Finally, significant age uncertainties may arise for time intervals between two tie points because of changing sediment accumulation rates.

5 Results and Discussion

5.1 Ti/Ca and Zr/Rb as proxies for terrigenous inputs and grain size

As defined by our age model construction, Ti/Ca values abruptly decrease (increase) in accord with onsets of Greenland stadials (interstadials), whereas Zr/Rb values show opposite trends (Fig. 4c-d). In particular, stadial events are characterized by (1) reduced Ti/Ca (or increased $CaCO_3$ content; Fig. 3c) and (2) increased Zr/Rb values, implying (1) reduction in terrigenous contributions versus marine carbonates and (2) sediment coarsening. The magnetic susceptibility record exhibits a similar pattern to that of Zr/Rb ratios, where grains are coarser, magnetic values are higher (Fig. 4d). Accordingly, earlier studies report that ferrimagnetic minerals, of which concentrations are reflected by the magnetic susceptibility, are associated with higher content of silt and sand-sized lithogenic components (Vanderaveroet et al., 1999; Shankar et al., 2006). In addition, stadial periods are characterized by reduced sedimentation rates (Fig. 4e). We note here that we focus on millennial-scale variability in the elemental proxy records rather than glacial-interglacial changes.

We use the Ti/Ca ratio to reconstruct changes in continental weathering and relative terrigenous contributions to the marine sediment record and, ultimately, variations in river run-off and northern South American rainfall. Elemental ratios including Ca, however, also depend on marine biogenic content (Govin et al., 2012). Thus there is a possibility that Ti/Ca patterns are affected by productivity changes and/or preservation of carbonate, which is mainly of biogenic origin derived from foraminifera, coccoliths, and pteropods (Reid et al., 1996). We suggest that reduced Ti/Ca (or increased $CaCO_3$ content) during stadial events cannot be related to increased marine productivity, because of opposite evidence from existing proxy records for productivity

(i.e., total organic carbon and faunal data) from core M35003-4 (Hüls & Zahn, 2000). A reduced stadial productivity is also further confirmed by high accumulation rates of oligotrophic calcareous dynocyst species (Vink et al., 2001). We note that productivity levels in the region today are controlled by Orinoco River discharge with maximum values during wet season and very low productivity values (comparable to estimations in oligotrophic waters) during dry season (Muller-Karger et al., 1988; Bonilla et al., 1993; López et al., 2013).

Dissolution may have affected the $CaCO_3$ amounts, biasing our interpretation of Ti/Ca to some degree. Indeed, based on fragmentation of planktic foraminifera in core M35003-4, Hüls & Zahn (2000) showed that carbonate dissolution was elevated during interstadial times. Thus, dissolution may have removed Ca, causing sediments to become enriched with terrigenous material when compared to stadial periods. Better carbonate preservation during stadials was possibly a result of reduced bottom water corrosiveness due to lowered flux of organic matter to the sea floor at times of reduced primary productivity (Reid et al., 1996). The dissolution cycles furthermore may have been caused by climate-controlled deep ocean circulation changes, including variations in the influence of the bottom currents (Gu et al., 2017). However, continuous contents of sensitive aragonite and high-magnesium-calcite (on average forming ~40 % and ~10 % and of the total $CaCO_3$, respectively, Hüls & Zahn, 2000) suggest only limited dissolution in our core which at present is located well above calcite and aragonite lysoclines (Vink et al., 2001).

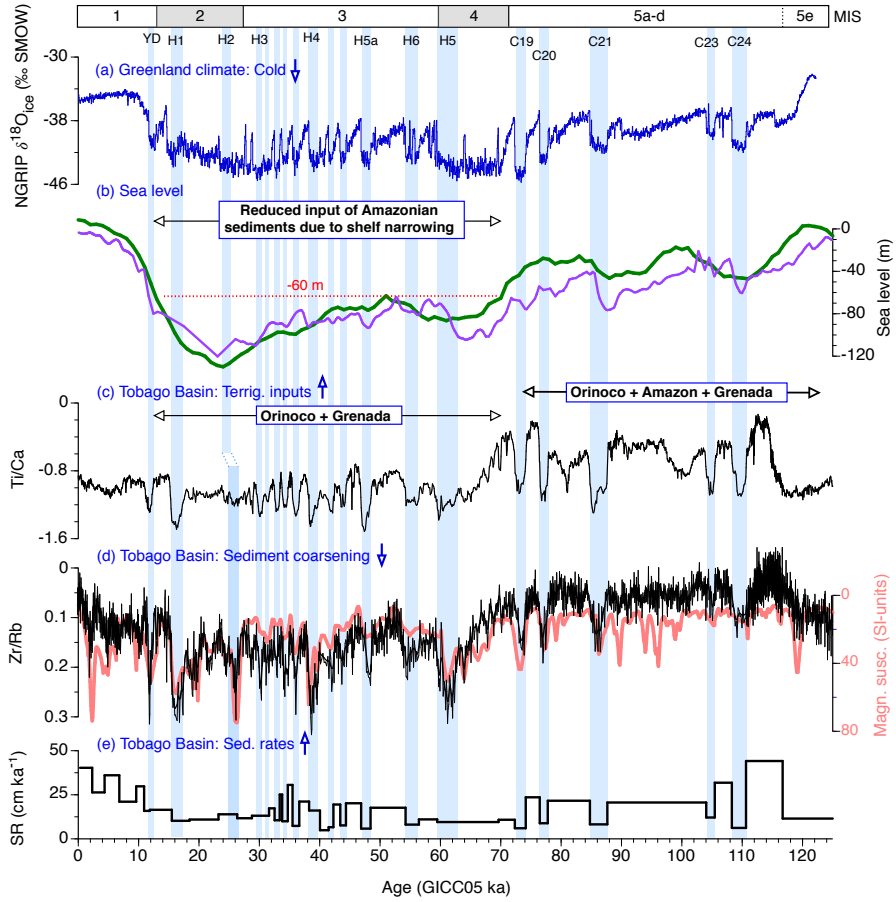

Figure 4. Proxy data from core MD99-2198 over past 125 ka compared to **(a)** Greenland ice $\delta^{18}O$ record (NGRIP Members, 2004) and **(b)** global sea level (green - Spratt & Lisiecki, 2016**,** violet – Grant et al., 2012). Proxy data from core MD99-2198 include **(c)** log-ratios of Ti/Ca, **(d)** log-ratios of Zr/Rb (original and smoothed; black) and magnetic susceptibility record (red; Labeyrie & Zahn, 2005a, b), and **(e)** sedimentation rates (SR). Blue boxes represent events of reduced terrigenous inputs / increased sediment coarsening in the Tobago Basin that are in phase with Greenland stadials. Labeled are YD – Younger Dryas, H1-H6 – Heinrich Stadials 1-6 and C19-21, C23-24 – Cold events in the North Atlantic during MIS 5. MIS – marine isotope stage.

390 We therefore argue that the dilution of marine carbonate by terrigenous material had a
391 primary effect on the Ti/Ca ratios. First, stadial events, characterized by higher carbonate content,
392 exhibit reduced sedimentation rates (Fig. 4e), suggesting relative reduction in terrigenous input.
393 Second, our Ti/Ca record strongly correlates with Zr/Rb (R=-0.8 during the last glacial period,
394 MIS 2-5d); the latter is a well-established proxy for grain size of lithogenic particles (Chen et al.,
395 2006; Phillips et al., 2015; Gebregiorgis et al., 2018). Zr/Rb ratios imply that stadial periods
396 contain coarser sediments (Fig. 4d), something that is confirmed by grain size data from core
397 M35003-4 (Hüls & Zahn, 2000). Sediment coarsening may be attributed to a reduced input of
398 distal material, finer sediment particles from the Orinoco and Amazon Rivers, and thus, to a
399 relative enrichment of proximal, coarser components from Grenada island (Fig. 2). Although we
400 cannot rule out a certain grain size variability as a result of changes in bottom water current
401 strength (e.g., Wu et al., 2020), the fluctuations in the amount of fluvial clay input should
402 completely mask the signal, especially during interstadials. Today clays from South American
403 rivers constitute about 20 % of sediments in the Tobago Basin (Reid et al., 1996). A reduced supply
404 of these sediments during stadials would explain coevally-found low sedimentation rates, the
405 sediment coarsening, and the low Ti/Ca. Thus we conclude that our Ti/Ca ratios can be used as a
406 robust indicator of millennial-scale variability in terrigenous inputs.
407
408 Terrigenous inputs in the Tobago Basin are strongly controlled by river discharges (Reid
409 et al., 1996). The run-off is linked with rainfall amounts in the Orinoco and Amazon Basins, related
410 to SAMS intensities and ITCZ movements (Fig. 1B). We note, however, that non-uniform
411 precipitation regimes over large catchment areas of Orinoco and Amazon Rivers (Poveda et al.,
412 2006) as well as various geology (Edmond et al., 1995; Rousseau et al., 2019) can complicate

413 interpretations of our elemental records. In addition, amounts of fluvial (and terrigenous) material
414 in our core can be influenced by other factors, such as changes in sea level, ocean currents,
415 prevailing winds, and vegetation cover**.** The roles of these factors will be discussed below.
416
417 *5.2 D-O cycles during MIS 5a-5d: Amazonian influence and implications for the NBC strength*
418 As pointed out above, the analogous sedimentary changes, i.e., reduced terrigenous inputs
419 (low Ti/Ca), sediment coarsening (high Zr/Rb) and lowered sedimentation rates characterized
420 stadial events in our core during both MIS 2-4 and MIS 5a-5d (Fig. 4). This is noteworthy, since
421 MIS 2-4 and MIS 5a-5d were marked by contrasting sedimentary regimes caused by different sea
422 level stands. In particular, the supply of Amazonian sediments to the Caribbean Sea was strongly
423 reduced during time intervals characterized by sea level lower than -60 m, such as MIS 2-4
424 (Fig. 4b; Schlünz et al., 1999). In contrast, during interglacial sea level high stands the Amazon
425 River is the main source for fine-grained material in the nearshore areas off northern South
426 America (Milliman et al., 1982; Bowles & Fleischer, 1985; Govin et al., 2014). It was shown that
427 ~80% of the particularly fine-grained material (<2 μm) in the present-day Gulf of Paria (Fig. 2) is
428 sourced from the Amazon River, while the rest is Orinoco-derived (Eisma et al., 1978; Milliman
429 et al., 1982). It is noteworthy that the grain size of Amazonian sediments delivered towards the
430 continental slope of the northeastern South America remained unaffected by the millennial-scale
431 precipitation changes (e.g., Kanner et al., 2012), possibly due to a blurring effect by the long
432 transport way from the eastern Andes to the Atlantic Ocean (Zhang et al., 2015b; 2017).
433
434 Unlike MIS 2-4, MIS 5a-5d was characterized by a sea level stand between -20 m and -
435 60 m (Fig. 4b; Grant et al., 2012; Spratt & Lisiecki, 2016). Thus, input of fine-grained Amazonian

436 sediments could be expected. This is especially relevant during stadial events due to inferred
437 increased humidity in the western Amazonia (Fig. 5a; Mosblech et al., 2012; Cheng et al., 2013),
438 which is the main source area for present-day Amazonian sediments (Filizola et al., 2011; Govin
439 et al., 2014). Instead, reduced terrigenous inputs (low Ti/Ca), sediment coarsening (high Zr/Rb),
440 and lowered sedimentation rates characterize these stadial events in our sediment core (Fig. 5c and
441 4e), suggesting reduced fluvial inputs from both the Orinoco and the Amazon rivers. Lowered
442 input of Orinoco-derived material during stadial events can be explained by more arid conditions
443 in the northern South America (see 5.3). Concurrently, reduced supply of Amazonian sediments
444 may be the result of stadial-interstadial reorganization of ocean surface currents (see below).
445
446 Following earlier studies, we attribute the reduced Amazonian sediment delivery to our
447 core site during stadial events of MIS 5a-5d to a weakened transport of the NBC, caused by reduced
448 AMOC strength (Chang et al., 2008; Schmidt et al., 2012; Nace et al., 2014; Zhang et al., 2015b;
449 Mulitza et al., 2017). This conclusion is supported by paleo-reconstructions off the northeastern
450 Brazil margin. In core GL-1248, elevated Ti/Ca values during Heinrich and stadial periods were
451 associated with increased deposition of terrigenous detritus linked with an AMOC-related
452 reduction in the NBC transport that coincided with increased precipitation on the adjacent land
453 (Figs. 1 and 5b; Venancio et al., 2018). The latter is supported by data from a nearby core CDH-
454 86 (Figs. 1 and 5b). There, high Fe/K values during stadials point to a more intense chemical
455 wheathering that resulted in elevated concentrations of iron relative to more soluble and mobile
456 potassium (Nace et al., 2014).

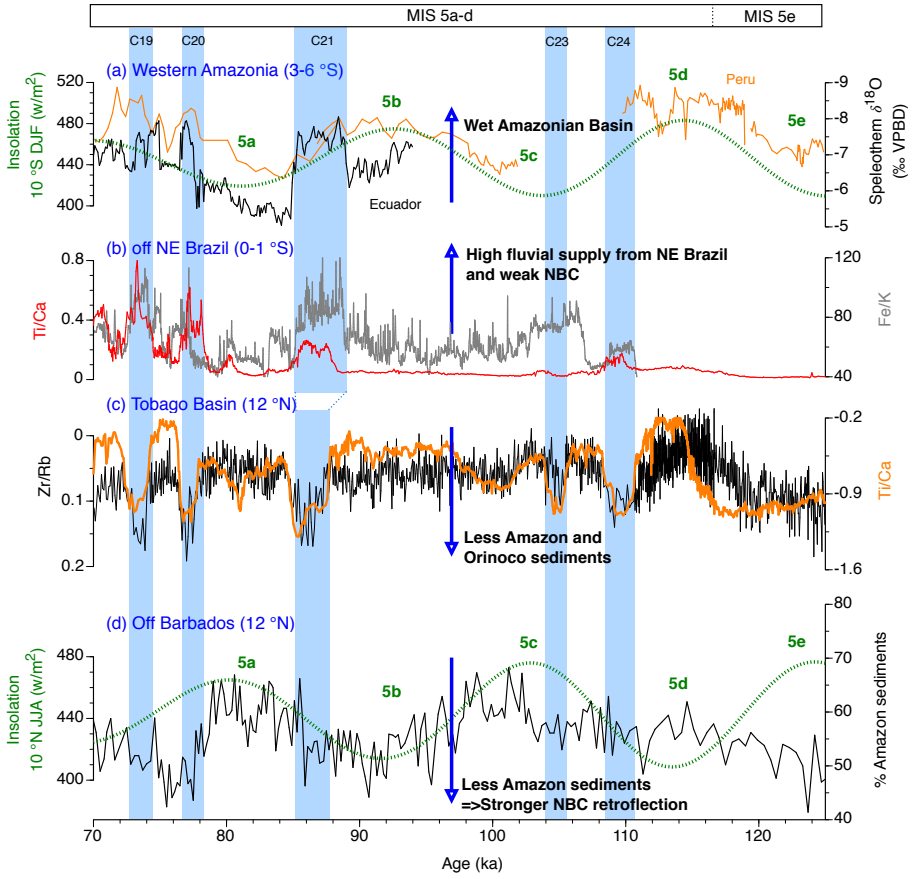

Figure 5. Proxy data comparison during MIS 5. **(a)** Speleothem $\delta^{18}O$ values from Santiago Cave, Ecuador (black; Mosblech et al., 2012) and Cueva del Diamante Cave, Peru (orange; Cheng et al., 2013), **(b)** Ti/Ca values in core GL-1248 (red; Venancio et al., 2018) and smoothed (5-point moving average) Fe/K values in core CDH-86 (grey; Nace et al., 2014), both retrieved off the NE Brazil margin, **(c)** log-ratios of Zr/Rb (black) and Ti/Ca (orange) from core MD99-2198 retrieved from the Tobago Basin (this study), **(d)** percentage of Amazon material within the terrigenous fraction in core GeoB3938-1 retrieved off Barbados (Govin et al., 2014). Also shown are **(d)** boreal summer (JJA) insolation at 10 °N and **(a)** austral summer insolation (DJF) at 10 °S (Laskar et al., 2004). Blue boxes represent events of reduced terrigenous inputs / increased sediment coarsening in the Tobago Basin that are in phase with Greenland stadials. Labeled are C19-21, C23-24 – Cold

events in the North Atlantic during MIS 5, 5a-5e – substages of MIS 5. MIS – marine isotope stage.

Although surface inflows from the South Atlantic near our sediment core location are essentially AMOC-driven (Johns et al., 2002), changes of the tropical atmospheric system could have influenced the overall strength of the NBC (Johns et al., 1998; Rodriguez et al., 2007), thereby also affecting the amounts of Amazonian sediments transported towards the Tobago Basin. By analogy to the modern situation in boreal winter (Johns et al., 1998), intensified northeastern trade winds during stadial events (Collins et al., 2011) accompanied by an asymmetric weakening of the southeastern trade winds (McGee et al., 2018) could have caused a reduction in the NBC current transport (Venancio et al., 2018). Moreover, wind-related strengthening (weakening) of the NBC retroflection could have caused more (less) Amazonian sediments to be deflected into the open ocean (Rühlemann et al., 2001; Wilson et al., 2011). For instance, a sediment core GeoB3938-1 retrieved off Barbados (Fig. 1) reveals lowered input of Amazon versus Orinoco-derived sediments during MIS 5b and MIS 5d (Fig. 5d; Govin et al., 2014), i.e., at times of increased Amazon precipitation aligned with austral summer insolation peaks (Fig. 5a; Cheng et al., 2013). Govin et al. (2014) further argue for a redistribution of Amazonian sediments by surface currents, implying intensification of the NBC retroflection during colder substages MIS 5b and MIS 5d. However, on millennial timescales, existing records do not reveal changes that can be readily ascribed to varations in the strength of the NBC retroflection (Fig. 5d), meaning that further work is needed to clarify the role of the NBC retroflection in stadial-interstadial climate dynamics (e.g., Piacsek et al., 2021).

491 *5.3 D-O cycles during MIS 2-4: Orinoco versus Grenada influence*

492 During MIS 2-4, when the sea level dropped below -60 m (Fig. 4b), wide parts of the
493 Guiana shelf in front of the Orinoco River as well as the Grenada shelf became exposed (Fig. 2).
494 Significant shelf narrowing during MIS 2-4 could have led to increased shelf-edge deposition of
495 the Amazonian sediments during its transport towards the Orinoco Delta (Bowles & Fleischer,
496 1985). These particularly fine-grained sediments today comprise half of material deposited along
497 the Orinoco coast (Warne et al., 2002) and their reduced supply during MIS 2-4 potentially
498 explaines the overall reduction in terrigenous inputs (low Ti/Ca), sediment coarsening (high Zr/Rb)
499 and lowered sedimentation rates (Fig. 4c-e). It is possible that some amounts of Amazonian
500 suspended material could have been still transported northwards by outer shelf currents (Bowles
501 & Fleischer, 1985; Govin et al., 2012), as suggested by the neodymium isotopic composition of
502 sediments off French Guiana (7 °N; Zhang et al., 2015b, 2017). However, a strong reduction in
503 the northward propagation of Amazonian material during MIS 2-4 is corroborated by lowered
504 sedimentation rates in the Guiana Basin, receving sediments prefentially from the Amazon River
505 (López-Otálvaro et al., 2013; Rama-Corredor et al., 2015). This is in agreement with earlier studies
506 showing that a sea-level drop of 40-60 m below the present-day is particularly critical, as it
507 activates accumulation of sediments on the Amazon deep sea fan (Schlünz et al., 1999; Rühlemann
508 et al., 2001; Maslin et al., 2006).

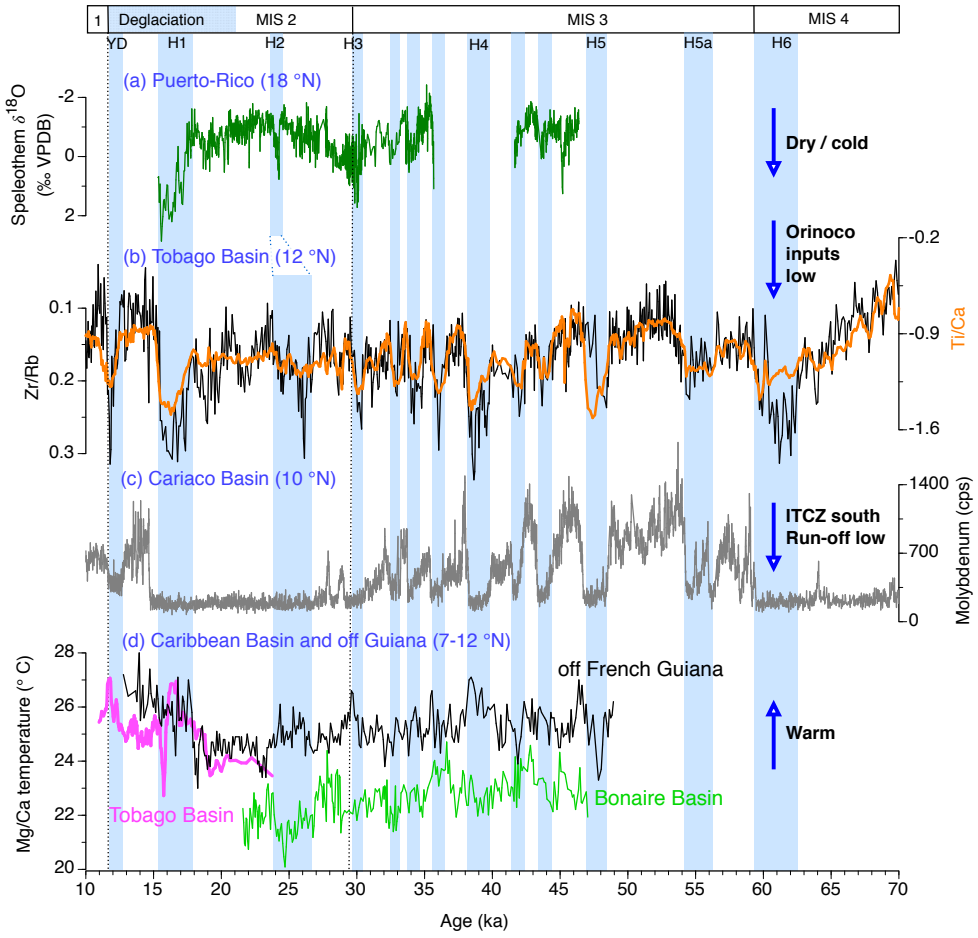

Figure 6. Proxy data comparison during MIS 2-4. **(a)** Speleothem $\delta^{18}O$ values from Larga Cave, Puerto-Rico (Warken et al., 2020), **(b)** log-ratios of Zr/Rb (black) and Ti/Ca (orange) from core MD99-2198 retrieved from the Tobago Basin (this study), **(c)** sedimentary molybdenum from core MD03-2622 obtained from the Cariaco Basin (Gibson & Peterson, 2014), **(d)** smoothed (5-point moving average) Mg/Ca-based water temperature reconstructions from core M78/1-235-1 retrieved from the Tobago Basin (magenta; Bahr et al., 2018), core VM12-107 from the Bonaire Basin (green; Parker et al., 2015) and core GeoB16224-1 off French Guinana (black; Crivellari et al., 2019). Blue boxes represent events of reduced terrigenous inputs / increased sediment coarsening in the Tobago Basin that are in phase with Greenland stadials. Labeled are YD – Younger Dryas, H1-H6 – Heinrich Stadials 1-6. MIS – marine isotope stage.

If during MIS 2-4 northward transport of Amazonian sediments was strongly reduced, stadial-interstadial Ti/Ca and Zr/Rb shifts in the our core record were mainly driven by changing terrigenous inputs from the Orinoco River (Fig. 6b). We note that increased input of Saharan dust – although plausible during stadial periods (Collins et al., 2011) – cannot explain sediment coarsening observed during these time intervals, as dust transported by the easterly trade winds towards the Caribbean is preferentially within the clay size range (Reid et al., 1996; Muhs et al., 2007). To explain coeval reductions in terrigenous inputs (low Ti/Ca), increased grain size (high Zr/Rb) and low sedimentation rates during stadial events, we therefore suggest reduced fluvial inputs from the Orinoco River to have caused the relative enrichment in coarser-grained proximal material from Grenada. Hence our results point to reduced (increased) rainfall in northern South America during stadial (interstadial) events which was linked with southern (northern) shifts of the mean annual position of the ITCZ. We further suggest that during stadial events, southward shifts of the ITCZ were associated with a strengthening of the northeastern trade winds (McGee et al., 2018) which brought moisture southwards (i.e., towards Amazon Basin; Baker et al., 2009) and suppressed the SAMS intensities in the northern South America. These inferences are in good agreement with earlier reconstructions from various circum-Caribbean regions, such as from the Central American lowlands (Hodell et al., 2008; Correa-Metrio et al., 2012**;** Escobar et al., 2012; Caballero et al., 2019), northern Mexico (Roy et al., 2013), Cuba (Warken et al., 2019) and Puerto Rico (Fig. 6a; Warken et al., 2020).

The nearby Cariaco Basin has proven to be a unique location to study meridional climate teleconnections and precipitation fluctuations in the northern South America (Peterson et al., 2000; Deplazes et al., 2013; Gibson & Peterson, 2014). In particular, records of sedimentary

543 molybdenum from core MD03-2622 (Fig. 2) reveal abrupt fluctuations during MIS 3 which can
544 be associated with changes in productivity and river run-off (Fig. 6c): Interstadials (stadials) are
545 characterized by enriched (depleted) molybdenum, implying anoxic (oxygenated) conditions in
546 the basin, associated with high (low) productivity, high (low) riverine input, and a northerly
547 (southerly) shifted ITCZ (Gibson & Peterson, 2014). Good coherence with our Ti/Ca record (Fig.
548 6b) further supports our interpretation of the ITCZ-related change in precipitation over the Orinoco
549 River catchment area, in particular, the northern Andes, since this region provides the majority of
550 the river sediment load (Warne et al., 2002). Southward shifts in the position of the ITCZ are
551 further confirmed by dated speleothem and marine records from both sides of the equator (Wang
552 et al., 2007; Kanner et al., 2012; Corrick et al., 2020; Hughen & Heaton, 2020; Warken et al.,
553 2020). We note that sedimentary molybdenum in Cariaco core MD03-2622 is a threshold proxy
554 that under oxygenated conditions does not show a response. This explains strongly depleted
555 molybdenum values during most of MIS 2 and 4 (Fig. 6c), suggesting constantly oxygenated
556 conditions that could be ascribed to a far southern position of the ITCZ (Peterson et al., 2000;
557 Gibson & Peterson, 2014; Roberts & Hopcroft, 2020).
558
559 Our Zr/Rb record reveals a pronounced coarse-grained event during MIS 2, probably
560 coeval with H2 (Fig. 6b). Earlier studies suggested that during sea-level lowstand of MIS 2 inputs
561 from Grenada were particularly enhanced, while sediments from the Orinoco/Amazon Rivers were
562 mostly transported down to the Orinoco/Amazon Fans and the abyssal plain (Faugères et al., 1993;
563 Schlünz et al., 1999, 2000; Maslin et al., 2006; Deville et al., 2015). Change in the bottom currents
564 velocities and, thus, the AMOC vigor – today our core is influenced by the southward-flowing
565 upper North Atlantic Deep Water (NADW) originated in the northwestern North Atlantic

(Lambelet et al., 2016) - could have affected the grain size distribution during H2 event. However, some reconstructions suggest little or no change in AMOC strength during H2, as a result of a generally weak AMOC mode during MIS 2 (Lynch-Stieglitz et al., 2014; Parker et al., 2015). It is possible therefore that changing vegetation cover added to the observed changes in sediment grain size, at least during H2. While today the humid tropical climate of Grenada fosters a lush rainforest and evergreen vegetation (Ternan et al., 1989), a reduction in vegetation cover during colder North Atlantic events is very plausible (Clapperton, 1993; Escobar et al., 2012; Correa-Metrio et al., 2012).

5.3 High-to-low latitude teleconnections during D-O climate variability

We suggest that on millennial timescales sedimentary processes in the Tobago Basin were mainly controlled by variations in sedimentary load of rivers and hence by SAMS intensities in the northern South America. Sensitive to land-sea thermal contrasts, SAMS responded to insolation changes on orbital timescales (Cruz et al., 2009) and was likely intensified in the northern Andes during early Holocene (Hoffmann et al., 2014). It was further shown that SAMS is indirectly influenced by migration of the maritime ITCZ (Vuille et al., 2002; Baker et al., 2009) and associated strengthening/relaxation of trade winds (McGee et al., 2018). The ITCZ location is linked with the inter-hemispheric SST gradients, and it is generally accepted that during D-O cycles the ITCZ moved in reponse to switches in the AMOC strength and associated northward heat transport (Broccoli et al., 2006; Chiang & Friedmann, 2012). Crucially, there is strong evidence supporting the importance of the atmosphere in communicating the high-latitude cooling southwards and causing shifts in the ITCZ position (Chiang and Bitz, 2005; Timmermann et al., 2005; Chiang et al., 2008). Thus, the dominant hypothesis for the synchrony between the abrupt

589 tropical precipitation changes and D-O temperature variations on Greenland is the fast (seasonal
590 to decadal timescales) atmospheric teleconnection (Liu & Alexander, 2007; Markle et al., 2017;
591 Corrick et al., 2020). In our core records, this coupling between high and low latitudes is especially
592 apparent during MIS 3, when fluvial sediments were predominantly supplied from the Orinoco
593 Basin located in the northernmost South America, particularly sensitive to the ITCZ shifts (Warne
594 et al., 2002). In contrast, during the D-O cycles of MIS 5a-5d, influence from the ocean surface
595 currents could have also influenced the sedimentation process (i.e., redistribution of Amazonian
596 sediments, see 5.2).
597
598 Proxy data and climate models indicate that changes in the AMOC strength were involved
599 in the D-O variability during the last glacial period (Henry et al., 2016; Burckel et al., 2015;
600 Gottschalk et al., 2015; Zhang et al., 2015a; Them et al., 2015) and possibly, but not necessarily,
601 also during MIS 5 (Thornalley et al., 2013; Böhm et al., 2015; Lynch-Stieglitz, 2017). During
602 stadial events, the AMOC strength was weak and northward transport of heat was reduced,
603 resulting in cooling in the North Atlantic and warming in the South Atlantic through the bipolar
604 seesaw mechanism (Stocker & Johnson, 2003; Barker et al., 2009). Earlier studies indicated that
605 the fulcrum of the bipolar seesaw was located in the subtropical North Atlantic (Zarriess et al.,
606 2011). However, more recent studies show that the actual seesaw that developed was between the
607 sea surface in the high northern latitudes and the polar atmosphere, which cooled during times of
608 AMOC slowdown, and the subsurface and intermediate waters in the North and South Atlantic,
609 which warmed (Weldeab et al., 2006; Barker et al., 2009**;** Marcott et al., 2011; Ezat et al., 2014;
610 Nace et al., 2014; Rasmussen et al., 2016; Crivellari et al., 2018, 2019; Pedro et al., 2018; Sessford
611 et al., 2019). Variations in the interhemispheric heat redistribution via the AMOC are further

612 invoked to explain the bipolar seesaw relationship between Greenland and Antarctica temperatures
613 (Fig. 7a and d; Stocker & Johnson, 2003; EPICA Community Members, 2006; Barker et al., 2009).

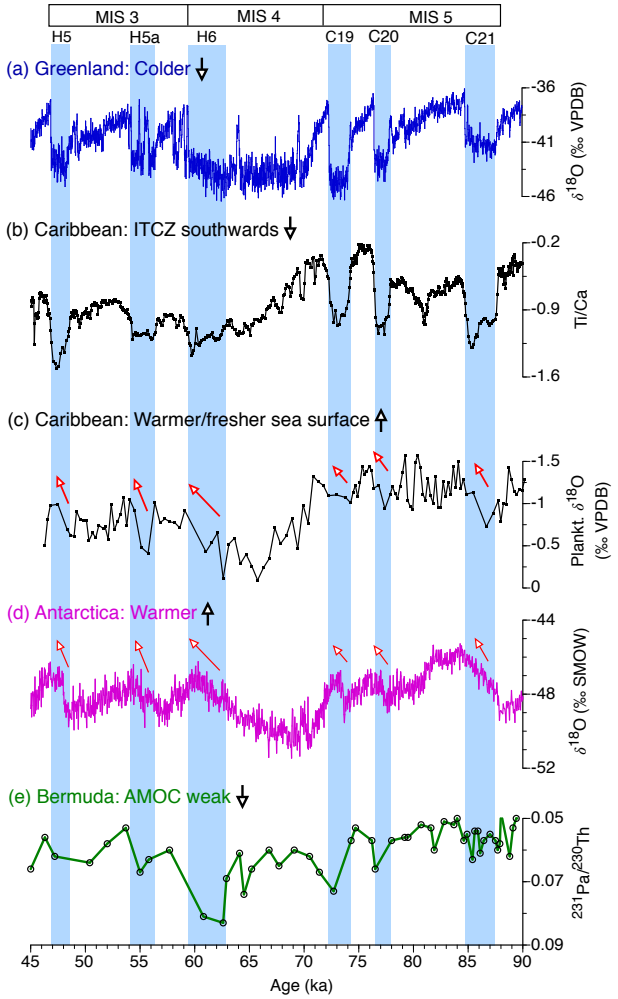

614

615 **Figure 7.** Comparison of proxy records from high and low latitudes during MIS 3-5. **(a)** Greenland
616 ice $\delta^{18}O$ record on GICC05 timescale (NGRIP Members, 2004; Rasmussen et al., 2014), **(b)** Log-
617 ratios of Ti/Ca in core MD99-2198 (this study), **(c)** $\delta^{18}O$ values in *G. ruber* (white) in core MD99-
618 2198 (Griffiths et al., 2013), **(d)** Antarctica ice core EDML $\delta^{18}O$ record on AICC2012 chronology
619 (EPICA Community Members, 2006; Bazin et al., 2013), **(e)** $^{231}Pa/^{230}Th$ data from ODP Site 1063
620 retrieved from the Bermuda Rise (Böhm et al., 2015). Blue boxes represent events of reduced
621 terrigenous inputs in the Tobago Basin that are in phase with Greenland stadials. Note that $\delta^{18}O$

values in *G. ruber* (white) in the southeastern Caribbean Sea **(c)** correlate with Antarctica temperatures **(d)** and therefore sea surface properties could be influenced by the bipolar seesaw and the AMOC. Labeled are H5-H6 – Heinrich Stadials 5-6 and C19-21 – Cold events in the North Atlantic during MIS 5. NH – northern hemisphere, MIS – marine isotope stage.

While existing high-resolution SST reconstructions from the Caribbean Basin go back to late MIS 3 (Fig. 6d; Schmidt et al., 2012; Parker et al., 2015; Bahr et al., 2018; Reißig et al., 2018), older climate intervals, such as early MIS 3 and MIS 4-5, remain less-studied. To address the latter in terms of millennial-scale ocean variability in the Tobago Basin we made use of the published *G. ruber* (white) $\delta^{18}O$ record by Griffiths et al. (2013). Comparing this record with our Ti/Ca values shows that significant reductions in $\delta^{18}O$ values occurred halfway through most stadial events, e.g., H5, H5a or C19-21 (Fig. 7b-c). We are aware that lower resolution of the $\delta^{18}O$ record may hinder further intepretations. However, we argue that in the context of millennial-scale climate variations our dataset clearly and consistently demonstrates lowering trends in $\delta^{18}O$ that precede abrupt Ti/Ca increases at the interstadial onsets. Because $\delta^{18}O$ values in shallow-dwelling species *G. ruber* (white) reflect combined temperature and salinity signal within the upper 50 m, the changes either imply sea surface freshening or warming during stadial events of MIS 3-5. We suggest that stadial $\delta^{18}O$ lowering was not driven by precipitation increase (~sea surface freshening), because of opposite evidence from the Cariaco Basin, showing that precipitation was at its lowest during the late phase of stadial events, due to a far southern position of the ITCZ (Deplazes et al., 2013). In addition, increased sea surface salinities were inferred in the subtropical to central western Atlantic during entire stadials (except perhaps their last centuries), as a result of diminished salt export via NADW in response to AMOC weakening (Schmidt et al., 2006;

645 Weldeab et al., 2006; Carlson et al., 2008; Bahr et al., 2013a, 2018) and/or due to enhanced tropical
646 aridity in conjuction with northeastern trade winds strengthening and ITCZ shifts (Schmidt &
647 Lynch-Stieglitz, 2011; Them et al., 2015).
648
649 If precipitation changes were not a major cause for stadial $\delta^{18}O$ reductions, these lowering
650 trends may be attributed to warming of the upper ocean in the Tobago Basin. Our results therefore
651 extend earlier findings in the region, noting SST rise during cold events in the high northern
652 latitudes (Rühlemann et al., 1999; Hüls & Zahn, 2000; Bahr et al., 2018). Following these studies,
653 it can be further argued that stadial warming in the Tobago Basin correlated with temperature
654 change in Antarctica (Fig. 7c-d). This, in turn, suggests that the interhemispheric ocean heat
655 redistribution via AMOC influenced the properties of the sea surface layer in the southeastern
656 Caribbean Sea and, importantly, not only during D-O events of the last glacial period, i.e., MIS 2-
657 4 (Hüls & Zahn, 2000), but also during the generally warmer MIS 5. Our data thus provide
658 evidence for changes in AMOC strength during stadials of MIS 5a-5d, which to some extent was
659 already indicated in $^{231}Pa/^{230}Th$ data from the Bermuda Rise (Böhm et al., 2015; Fig. 7e). These
660 inferences are further supported by Mg/Ca-derived SST reconstructions from marine sediment
661 cores further upstream from the NBC, off French Guinea (Fig. 6d; Crivellari et al., 2019) and off
662 northeastern Brazil (Nace et al., 2014). In agreement with modelling studies (Kageyama et al.,
663 2013), these records register a temperature increase during the majority of stadials and attribute
664 these warming trends to a reduced AMOC strength (Crivellari et al., 2019**)**.
665
666 Some modeling results indicate that stadial sea surface warming in the Tobago Basin may
667 originate from the upwelling of warmer subsurface waters (Wan et al., 2009; Schmidt et al., 2012).

668 Whereas no upwelling cell occurs in the actual Tobago Basin today, during glacial times as well
669 as probably during MIS 5, an upwelling cell likely existed in the basin fostered by reduced sea
670 level, east-west trending coastline and intensified northeastern trade winds (Hüls & Zahn, 2000;
671 Vink et al., 2001). Regardless of that, it would not strongly impede our interpretation, since the
672 proposed subsurface warming during stadial events was associated with AMOC weakening
673 causing a southward expansion of the subtropical gyre (Chang et al., 2008; Schmidt et al., 2012;
674 Parker et al, 2015; Reißig et al., 2018). Moreover, invoking subsurface (rather than surface)
675 warming would help to reconcile the contrasting temperature response to stadial conditions (i.e.,
676 cooling) registered in speleothems from Guatemala (Correa-Metrio et al., 2012) and Bahamas
677 (Arienzo et al., 2015), and in lacustrine sediments from Mexico (Caballero et al., 2019); possibly
678 these records reflect atmosphere-induced cooling during stadials due to strengthening of the
679 northeastern trades (Chiang et al., 2003, 2008; Wan et al., 2009). Considering the inferred
680 sensitivity of western tropical Atlantic to AMOC changes, more multi-proxy studies like our are
681 warranted to better understand the systematics behind the larger-scale ocean-atmosphere
682 interactions. In this context, the high-resolution Ti/Ca record presented by us, which mainly
683 reflects abrupt precipitation-driven sedimentary changes in temporal accord with D-O cycles on
684 Greenland, seems also a viable mean for regional core-to-core correlations.
685

686 **6 Conclusions**

687 Our high-resolution Ti/Ca record from the Tobago Basin reveals millennial-scale D-O
688 variability in relation with hydroclimate of northern South America. Stadial events were
689 characterized by low Ti/Ca ratios and high Zr/Rb values, reflecting reduced deposition of fine-
690 grained material from the Orinoco and Amazon Rivers. During MIS 3, the overall delivery of the

691 Amazonian sediments towards the Tobago Basin was diminished due to sea level lowstand and
692 shelves exposure. Therefore, reductions in the Orinoco River discharge during stadial events can
693 explain lowered deposition of fine-grained terrigenous material. During MIS 5a-5d, reduced
694 influence from both the Orinoco and the Amazon Rivers is suggested. We further propose that a
695 weakened NBC, a result of AMOC disturbances and/or atmospheric reorganisations, can explain
696 the diminished supply of the Amazonian sediments during stadial events of MIS 5a-5d.
697
698 Abrupt shifts in our Ti/Ca record were presumably coeval with Greenland
699 stadials/interstadial transitions due to rapid high-to-low-latitudes atmospheric reorganizations
700 involving shifts in the ITCZ. Furthermore, based on $\delta^{18}O$ values, we speculate that upper ocean in
701 the Tobago Basin warmed during several stadials of MIS 3-5. That inferred warming is out of
702 phase with temperature changes in the high northern latitudes, but correlates with temperature
703 development in Antarctica. Therefore, we argue that the ocean properties were influenced by the
704 bipolar seesaw and thus AMOC variations, and importantly, not only during the last glacial period,
705 but also during abrupt climate change of the generally warmer MIS 5.
706
707 **Acknowledgments**
708 S. Müller and D. Garbe-Schönberg are thanked for technical support during XRF scanning at Kiel
709 University. We thank S. Barker and J. Griffiths for making data from core MD99-2198 available
710 for this study. P. Baker is acknowledged for providing data from core CDH-86. We thank two
711 anonymous reviewers for their comments which helped to considerably improve the manuscript.
712 The study acknowledges funding from German Research Foundation (DFG grants BA1367/12-1
713 and TI240/8-2). The data reported in this paper will be accessible through Pangaea.de by the time

714 the article is accepted. For the purposes of the peer review the data can be accessed in Zenodo.org
715 (https://doi.org/10.5281/zenodo.4590356).
716

717 **References**

718 Amante, C. & Eakins, B.W., 2009. ETOPO1 1 arc-minute global relief model: Procedures, data
719 sources and analysis. NOAA Technical Memorandum NESDIS NGDC-24. National
720 Geophysical Data Center, NOAA, doi:10.7289/V5C8276M [08.11.2020].
721 Arienzo, M.M., Swart, P.K., Pourmand, A., Broad, K., Clement, A.C., Murphy, L.N., Vonhof,
722 H.B., Kakuk, B., 2015. Bahamian speleothem reveals temperature decrease associated with
723 Heinrich stadials. Earth Planet. Sci. Lett. 430, 377–386.
724 https://doi.org/10.1016/j.epsl.2015.08.035.
725 Armijos, E., Crave, A., Espinoza, J.C., Filizola, N., Espinoza-Villar, R., Ayes, Fonseca, P., Fraizy,
726 P., Gutierrez, O., Vauchel, P., Camenen, B., Martiınez, J.M., Dos Santos, A., Santini, W.,
727 Cochonneau, G., Guyot, J.L., 2020. Rainfall control on Amazon sediment flux: synthesis
728 from 20 years of monitoring. Environ. Res. Comm. 2, 051008.
729 https://doi.org/10.1088/2515-7620/ab9003.
730 Bahr, A., Hoffmann, J., Schönfeld, J., Schmidt, M.W., Nürnberg, D., Batenburg, S.J., Voigt, S.,
731 2018. Low-latitude expressions of high-latitude forcing during Heinrich Stadial 1 and the
732 Younger Dryas in northern South America. Glob. Planet. Change 160, 1–9.
733 https://doi.org/10.1016/j.gloplacha.2017.11.008.
734 Bahr, A., Jiménez-Espejo, F.J., Kolasinac, N., Grunert, P., Hernández-Molina F. Javier, Röhl
735 Ursula, Voelker Antje H. L., Escutia Carlota, Stow Dorrik A. V., Hodell David, Alvarez-
736 Zarikian Carlos A., 2014. Deciphering bottom current velocity and paleoclimate signals
737 from contourite deposits in the Gulf of Cádiz during the last 140 kyr: An inorganic

738 geochemical approach. Geochem. Geophys. Geosyst. 15, 3145–3160.
739 https://doi.org/10.1002/2014GC005356.
740 Bahr, A., Nürnberg, D., Karas, C., Grützner, J., 2013a. Millennial-scale versus long-term dynamics
741 in the surface and subsurface of the western North Atlantic Subtropical Gyre during Marine
742 Isotope Stage 5. Glob. Planet. Change 111, 77–87.
743 https://doi.org/10.1016/j.gloplacha.2013.08.013.
744 Baker, P.A., Fritz, S.C., 2015. Nature and causes of Quaternary climate variation of tropical South
745 America. Quat. Sci Rev. 124, 31–47. https://doi.org/10.1016/j.quascirev.2015.06.011.
746 Baker, P.A., Fritz, S.C., Burns, S.J., Ekdahl, E., Rigsby, C.A., 2009. The nature and origin of
747 decadal to millennial scale climate variability in the southern tropics of South America. In:
748 Vimeux, F., Sylvestre, F., Khodri, M. (Eds.), Past Climate Variability from the Last Glacial
749 Maximum to the Holocene in South America and Sur- rounding Regions. Springer, NY,
750 pp. 301-322.
751 Barker, S., Diz, P., Vautravers, M.J., Pike, J., Knorr, G., Hall, I.R., Broecker, W.S., 2009.
752 Interhemispheric Atlantic seesaw response during the last deglaciation. Nature 457, 1097–
753 1102. https://doi.org/10.1038/nature07770.
754 Bazin, L., Landais, A., Lemieux-Dudon, B., Toyé Mahamadou Kele, H., Veres, D., Parrenin, F.,
755 Martinerie, P., Ritz, C., Capron, E., Lipenkov, V., Loutre, M.-F., Raynaud, D., Vinther, B.,
756 Svensson, A., Rasmussen, S.O., Severi, M., Blunier, T., Leuenberger, M., Fischer, H.,
757 Masson-Delmotte, V., Chappellaz, J., Wolff, E., 2013. An optimized multi-proxy, multi-
758 site Antarctic ice and gas orbital chronology (AICC2012): 120–800 ka. Clim. Past 9, 1715–
759 1731. https://doi.org/10.5194/cp-9-1715-2013.

760 Blaauw, M., Christen, J.A., 2011. Flexible paleoclimate age-depth models using an autoregressive
761 gamma process. Bayesian Anal. 6, 457–474. https://doi.org/10.1214/11-BA618.
762 Böhm, E., Lippold, J., Gutjahr, M., Frank, M., Blaser, P., Antz, B., Fohlmeister, J., Frank, N.,
763 Andersen, M.B., Deininger, M., 2015. Strong and deep Atlantic meridional overturning
764 circulation during the last glacial cycle. Nature 517, 73.
765 https://doi.org/10.1038/nature14059.
766 Bond, G., Broecker, W., Johnsen, S., McManus, J., Labeyrie, L., Jouzel, J., Bonani, G., 1993.
767 Correlations between climate records from North Atlantic sediments and Greenland ice.
768 Nature 365, 143–147. https://doi.org/10.1038/365143a0.
769 Bonilla, J., Senior, W., Bugden, J., Zafiriou, O., Jones, R., 1993. Seasonal distribution of nutrients
770 and primary productivity on the eastern continental shelf of Venezuela as influenced by the
771 Orinoco River. J. Geophys. Res.: Oceans 98, 2245-2257.
772 https://doi.org/10.1029/92JC02761.
773 Bowles, F.A., Fleischer, P., 1985. Orinoco and Amazon River sediment input to the eastern
774 Caribbean Basin. Mar. Geol. 68, 53–72. https://doi.org/10.1016/0025-3227(85)90005-2.
775 Broccoli, A. J., Dahl, K. A., Stouffer, R. J., 2006. Response of the ITCZ to Northern Hemisphere
776 cooling, Geophys. Res. Lett. 33, L01702, doi:10.1029/2005GL024546.
777 Burckel, P., Waelbroeck, C., Gherardi, J.M., Pichat, S., Arz, H., Lippold, J., Dokken, T., Thil, F.,
778 2015. Atlantic Ocean circulation changes preceded millennial tropical South America
779 rainfall events during the last glacial. Geophys. Res. Lett. 42, 411–418.
780 https://doi.org/10.1002/2014GL062512.
781 Caballero, M., Lozano-García, S., Ortega-Guerrero, B., Correa-Metrio, A., 2019. Quantitative
782 estimates of orbital and millennial scale climatic variability in central Mexico during the

783 last ~40,000 years. Quat. Sci Rev. 205, 62–75.
784 https://doi.org/10.1016/j.quascirev.2018.12.002.
785 Carlson, A.E., Oppo, D.W., Came, R.E., LeGrande, A.N., Keigwin, L.D., Curry, W.B., 2008.
786 Subtropical Atlantic salinity variability and Atlantic meridional circulation during the last
787 deglaciation. Geology 991–994. https://doi.org/doi.org/10.1130/G25080A.
788 Chang, P., Zhang, R., Hazeleger, W., Wen, C., Wan, X., Ji, L., Haarsma, R.J., Breugem, W.-P.,
789 Seidel, H., 2008. Oceanic link between abrupt changes in the North Atlantic Ocean and
790 the African monsoon. Nature Geosci. 1, 444–448. https://doi.org/10.1038/ngeo218.
791 Chen, J., Chen, Y., Liu, L., Ji, J., Balsam, W., Sun, Y., Lu, H., 2006. Zr/Rb ratio in the Chinese
792 loess sequences and its implication for changes in the East Asian winter monsoon strength.
793 Geochim. Cosmochim. Acta 70, 1471–1482. https://doi.org/10.1016/j.gca.2005.11.029.
794 Cheng, H., Sinha, A., Cruz, F.W., Wang, X., Edwards, R.L., d'Horta, F.M., Ribas, C.C., Vuille,
795 M., Stott, L.D., Auler, A.S., 2013. Climate change patterns in Amazonia and biodiversity.
796 Nat. Commun. 4, 1411. https://doi.org/10.1038/ncomms2415.
797 Chiang, J.C.H., Biasutti, M., Battisti, D.S., 2003. Sensitivity of the Atlantic Intertropical
798 Convergence Zone to Last Glacial Maximum boundary conditions. Paleoceanography 18.
799 https://doi.org/10.1029/2003PA000916.
800 Chiang, J.C.H., Bitz, C.M., 2005. Influence of high latitude ice cover on the marine Intertropical
801 Convergence Zone. Clim. Dyn. 25, 477–496. https://doi.org/10.1007/s00382-005-0040-5.
802 Chiang, J. C., Friedman, A. R., 2012. Extratropical cooling, interhemispheric thermal gradients,
803 and tropical climate change. Annu. Rev. Earth Planet. Sci., 40, 383-412.
804 https://doi.org/10.1146/annurev-earth-042711-105545.

805 Chiang, J.C.H., Cheng, W., Bitz, C.M., 2008. Fast teleconnections to the tropical Atlantic sector
806 from Atlantic thermohaline adjustment. Geophys. Res. Lett. 35.
807 https://doi.org/10.1029/2008GL033292.
808 Chiang, J.C.H., Kushnir, Y., Giannini, A., 2002. Deconstructing Atlantic Intertropical
809 Convergence Zone variability: Influence of the local cross-equatorial sea surface
810 temperature gradient and remote forcing from the eastern equatorial Pacific. J. Geophys.
811 Res. Atmos. 107, ACL 3-1. https://doi.org/10.1029/2000JD000307.
812 Clapperton, C.M., 1993. Nature of environmental changes in South America at the Last Glacial
813 Maximum. Palaeogeogr. Palaeoclimatol. Palaeoecol 101, 189–208.
814 https://doi.org/10.1016/0031-0182(93)90012-8.
815 Collins, J.A., Schefuß, E., Heslop, D., Mulitza, S., Prange, M., Zabel, M., Tjallingii, R., Dokken,
816 T.M., Huang, E., Mackensen, A., Schulz, M., Tian, J., Zarriess, M., Wefer, G., 2011.
817 Interhemispheric symmetry of the tropical African rainbelt over the past 23,000 years.
818 Nature Geosci 4, 42–45. https://doi.org/10.1038/ngeo1039.
819 Cook, K.H., 2009. South American climate variability and change: remote and regional forcing.
820 In: Vimeux, F., Sylvestre, F., Khodri, M. (Eds.), Past Climate Variability in South America
821 and Surrounding Regions. Springer, Netherlands, pp. 193-212.
822 Correa-Metrio, A., Bush, M.B., Cabrera, K.R., Sully, S., Brenner, M., Hodell, D.A., Escobar, J.,
823 Guilderson, T., 2012. Rapid climate change and no-analog vegetation in lowland Central
824 America during the last 86,000 years. Quat. Sci Rev. 38, 63–75.
825 https://doi.org/10.1016/j.quascirev.2012.01.025.
826 Corrick, E.C., Drysdale, R.N., Hellstrom, J.C., Capron, E., Rasmussen, S.O., Zhang, X.,
827 Fleitmann, D., Couchoud, I., Wolff, E., 2020. Synchronous timing of abrupt climate

828 changes during the last glacial period. Science 369, 963.
829 https://doi.org/10.1126/science.aay5538.
830 Crivellari, S., Chiessi, C.M., Kuhnert, H., Häggi, C., da Costa Portilho-Ramos, R., Zeng, J.-Y.,
831 Zhang, Y., Schefuß, E., Mollenhauer, G., Hefter, J., Alexandre, F., Sampaio, G., Mulitza,
832 S., 2018. Increased Amazon freshwater discharge during late Heinrich Stadial 1. Quat. Sci
833 Rev. 181, 144–155. https://doi.org/10.1016/j.quascirev.2017.12.005.
834 Crivellari, S., Chiessi, C.M., Kuhnert, H., Häggi, C., Mollenhauer, G., Hefter, J., Portilho-Ramos,
835 R., Schefuß, E., Mulitza, S., 2019. Thermal response of the western tropical Atlantic to
836 slowdown of the Atlantic Meridional Overturning Circulation. Earth Planet. Sci. Lett 519,
837 120–129. https://doi.org/10.1016/j.epsl.2019.05.006.
838 Cruz, F.W., Vuille, M., Burns, S.J., Wang, X., Cheng, H., Werner, M., Lawrence Edwards, R.,
839 Karmann, I., Auler, A.S., Nguyen, H., 2009. Orbitally driven east–west antiphasing of
840 South American precipitation. Nature Geosci. 2, 210–214.
841 https://doi.org/10.1038/ngeo444.
842 Dahl, K.A., Broccoli, A.J., Stouffer, R.J., 2005. Assessing the role of North Atlantic freshwater
843 forcing in millennial scale climate variability: a tropical Atlantic perspective. Clim. Dyn.
844 24, 325–346. https://doi.org/10.1007/s00382-004-0499-5.
845 Deplazes, G., Lückge, A., Peterson, L.C., Timmermann, A., Hamann, Y., Hughen, K.A., Röhl, U.,
846 Laj, C., Cane, M.A., Sigman, D.M., Haug, G.H., 2013. Links between tropical rainfall and
847 North Atlantic climate during the last glacial period. Nature Geosci. 6, 213–217.
848 https://doi.org/10.1038/ngeo1712.
849 Deville, E., Mascle, A., Callec, Y., Huyghe, P., Lallemant, S., Lerat, O., Mathieu, X., Padron de
850 Carillo, C., Patriat, M., Pichot, T., Loubrieux, B., Granjeon, D., 2015. Tectonics and

851 sedimentation interactions in the east Caribbean subduction zone: An overview from the
852 Orinoco delta and the Barbados accretionary prism. Mar. Pet. Geol. 64, 76–103.
853 https://doi.org/10.1016/j.marpetgeo.2014.12.015.
854 Edmond, J. M., Palmer, M. R., Measures, C. I., Grant, B., Stallard, R. F., 1995. The fluvial
855 geochemistry and denudation rate of the Guayana Shield in Venezuela, Colombia, and
856 Brazil. Geochim. Cosmochim. Acta 59, 3301-3325. https://doi.org/10.1016/0016-
857 7037(95)00128-M.
858 Eisma, D., Van Der Gaast, S.J., Martin, J.M., Thomas, A.J., 1978. Suspended matter and bottom
859 deposits of the Orinoco delta: Turbidity, mineralogy and elementary composition. Neth. J.
860 Sea Res. 12, 224–251. https://doi.org/10.1016/0077-7579(78)90007-8.
861 EPICA Community Members, Barbante, C., C., Barnola, J.-M., Becagli, S., Beer, J., Bigler, M.,
862 Boutron, C., Blunier, T., Castellano, E., Cattani, O., Chappellaz, J., Dahl-Jensen, D.,
863 Debret, M., Delmonte, B., Dick, D., Falourd, S., Faria, S., Federer, U., Fischer, H., Freitag,
864 J., Frenzel, A., Fritzsche, D., Fundel, F., Gabrielli, P., Gaspari, V., Gersonde, R., Graf, W.,
865 Grigoriev, D., Hamann, I., Hansson, M., Hoffmann, G., Hutterli, M.A., Huybrechts, P.,
866 Isaksson, E., Johnsen, S., Jouzel, J., Kaczmarska, M., Karlin, T., Kaufmann, P., Kipfstuhl,
867 S., Kohno, M., Lambert, F., Lambrecht, Anja, Lambrecht, Astrid, Landais, A., Lawer, G.,
868 Leuenberger, M., Littot, G., Loulergue, L., Lüthi, D., Maggi, V., Marino, F., Masson-
869 Delmotte, V., Meyer, H., Miller, H., Mulvaney, R., Narcisi, B., Oerlemans, J., Oerter, H.,
870 Parrenin, F., Petit, J.-R., Raisbeck, G., Raynaud, D., Röthlisberger, R., Ruth, U., Rybak,
871 O., Severi, M., Schmitt, J., Schwander, J., Siegenthaler, U., Siggaard-Andersen, M.-L.,
872 Spahni, R., Steffensen, J.P., Stenni, B., Stocker, T.F., Tison, J.-L., Traversi, R., Udisti, R.,
873 Valero-Delgado, F., van den Broeke, M.R., van de Wal, R.S.W., Wagenbach, D., Wegner,

874 A., Weiler, K., Wilhelms, F., Winther, J.-G., Wolff, E., EPICA Community Members,
875 2006. One-to-one coupling of glacial climate variability in Greenland and Antarctica.
876 Nature 444, 195–198. https://doi.org/10.1038/nature05301.
877 Escobar, J., Hodell, D.A., Brenner, M., Curtis, J.H., Gilli, A., Mueller, A.D., Anselmetti, F.S.,
878 Ariztegui, D., Grzesik, D.A., Pérez, L., Schwalb, A., Guilderson, T.P., 2012. A ~43-ka
879 record of paleoenvironmental change in the Central American lowlands inferred from
880 stable isotopes of lacustrine ostracods. Quat. Sci Rev. 37, 92–104.
881 https://doi.org/10.1016/j.quascirev.2012.01.020.
882 Ezat, M.M., Rasmussen, T.L., Groeneveld, J., 2014. Persistent intermediate water warming during
883 cold stadials in the southeastern Nordic seas during the past 65 k.y. Geology 42, 663–666.
884 https://doi.org/10.1130/G35579.1.
885 Faugères, J.C., Gonthier, E., Griboulard, R., Masse, L., 1993. Quaternary sandy deposits and
886 canyons on the Venezuelan margin and south Barbados accretionary prism. Mar Geology
887 110, 115–142. https://doi.org/10.1016/0025-3227(93)90109-9.
888 Fick, S.E., Hijmans, R.J., 2017. WorldClim 2: new 1km spatial resolution climate surfaces for
889 global land areas. Int. J. Climatol., 37, 4302-4315.
890 Filizola, N., Guyot, J. L., Wittmann, H., Martinez, J. M., de Oliveira, E., 2011. The significance
891 of suspended sediment transport determination on the Amazonian hydrological
892 scenario. Sediment Transp. Aquat. Environ., 45-64.
893 Frank, U., Nowaczyk, N.R., Frederichs, T., Korte, M., 2017. Palaeo- and rock magnetic
894 investigations on Late Quaternary sediments from low latitudes. I: geomagnetic
895 palaeosecular variation and relative palaeointensity records from the Tobago Basin,
896 Southeast Caribbean. Geophys. J. Int., 208, 1740–1755.
897 https://doi.org/10.1093/gji/ggw481.

898 Gebregiorgis, D., Giosan, L., Hathorne, E.C., Anand, P., Nilsson-Kerr, K., Plass, A., Lückge, A.,
899 Clemens, S.C., Frank, M., 2020. What Can We Learn From X-Ray Fluorescence Core
900 Scanning Data? A Paleomonsoon Case Study. Geochem. Geophys. Geosyst. 21,
901 e2019GC008414. https://doi.org/10.1029/2019GC008414.
902 Gibson, K.A., Peterson, L.C., 2014. A 0.6 million year record of millennial-scale climate
903 variability in the tropics. Geophys. Res. Lett. 41, 969–975.
904 https://doi.org/10.1002/2013GL058846.
905 Gottschalk, J., Skinner, L.C., Misra, S., Waelbroeck, C., Menviel, L., Timmermann, A., 2015.
906 Abrupt changes in the southern extent of North Atlantic Deep Water during Dansgaard–
907 Oeschger events. Nature Geosci. 8, 950–954. https://doi.org/10.1038/ngeo2558.
908 Govin, A., Capron, E., Tzedakis, P.C., Verheyden, S., Ghaleb, B., Hillaire-Marcel, C., St-Onge,
909 G., Stoner, J.S., Bassinot, F., Bazin, L., Blunier, T., Combourieu-Nebout, N., El Ouahabi,
910 A., Genty, D., Gersonde, R., Jimenez-Amat, P., Landais, A., Martrat, B., Masson-
911 Delmotte, V., Parrenin, F., Seidenkrantz, M.-S., Veres, D., Waelbroeck, C., Zahn, R., 2015.
912 Sequence of events from the onset to the demise of the Last Interglacial: Evaluating
913 strengths and limitations of chronologies used in climatic archives. Quat. Sci Rev. 129, 1–
914 36. https://doi.org/10.1016/j.quascirev.2015.09.018.
915 Govin, A., Chiessi, C.M., Zabel, M., Sawakuchi, A.O., Heslop, D., Hörner, T., Zhang, Y., Mulitza,
916 S., 2014. Terrigenous input off northern South America driven by changes in Amazonian
917 climate and the North Brazil Current retroflection during the last 250 ka. Clim. Past. 10,
918 843–862. https://doi.org/10.5194/cp-10-843-2014.
919 Govin, A., Holzwarth, U., Heslop, D., Ford Keeling, L., Zabel, M., Mulitza, S., Collins, J.A.,
920 Chiessi, C.M., 2012. Distribution of major elements in Atlantic surface sediments (36°N–

921 49°S): Imprint of terrigenous input and continental weathering. Geochem. Geophys.
922 Geosyst. 13. https://doi.org/10.1029/2011GC003785.
923 Grant, K.M., Rohling, E.J., Bar-Matthews, M., Ayalon, A., Medina-Elizalde, M., Ramsey, C.B.,
924 Satow, C., Roberts, A.P., 2012. Rapid coupling between ice volume and polar temperature
925 over the past 150,000 years. Nature 491, 744. https://doi.org/doi:10.1038/nature11593.
926 Griffiths, J.D., Barker, S., Hendry, K.R., Thornalley, D.J.R., van de Flierdt, T., Hall, I.R.,
927 Anderson, R.F., 2013. Evidence of silicic acid leakage to the tropical Atlantic via Antarctic
928 Intermediate Water during Marine Isotope Stage 4. Paleoceanography 28, 307–318.
929 https://doi.org/10.1002/palo.20030.
930 Gu, S., Liu, Z., Zhang, J., Rempfer, J., Joos, F., Oppo, D. W., 2017. Coherent response of Antarctic
931 Intermediate Water and Atlantic Meridional Overturning Circulation during the last
932 deglaciation: reconciling contrasting neodymium isotope reconstructions from the tropical
933 Atlantic. Paleoceanography 32, 1036-1053. https://doi.org/10.1002/2017PA003092.
934 Hammer, Ø., Harper, D.A., Ryan, P.D., 2001. PAST: Paleontological Statistics Software Package
935 for Education and Data Analysis. Palaeontologia Electronica, 4, 9 p.
936 Harris, I., Jones, P.D., Osborn, T.J., Lister, D.H., 2014. Updated high-resolution grids of monthly
937 climatic observations - the CRU TS3.10 Dataset. Int. J. Climatol., 34, 623-642.
938 https://doi.org/doi:10.1002/joc.3711.
939 Hemleben, C., Zahn, R., Meischner, D., 1998. Karibik 1996: Cruise No. 35/1 (April 18 - June 3,
940 1996), in METEOR Berichte 98-3, Leitstelle METEOR, Institut für Meereskunde der
941 Universität Hamburg, 208 pp.
942 Henry, L.G., McManus, J.F., Curry, W.B., Roberts, N.L., Piotrowski, A.M., Keigwin, L.D., 2016.
943 North Atlantic ocean circulation and abrupt climate change during the last glaciation.
944 Science 353, 470. https://doi.org/10.1126/science.aaf5529.

945 Hodell, D.A., Anselmetti, F.S., Ariztegui, D., Brenner, M., Curtis, J.H., Gilli, A., Grzesik, D.A.,
946 Guilderson, T.J., Müller, A.D., Bush, M.B., Correa-Metrio, A., Escobar, J., Kutterolf, S.,
947 2008. An 85-ka record of climate change in lowland Central America. Quat. Sci Rev. 27,
948 1152–1165. https://doi.org/10.1016/j.quascirev.2008.02.008.
949 Hoffmann, J., Bahr, A., Voigt, S., Schönfeld, J., Nürnberg, D., & Rethemeyer, J., 2014.
950 Disentangling abrupt deglacial hydrological changes in northern South America: Insolation
951 versus oceanic forcing. Geology, 42(7), 579-582. doi: https://doi.org/10.1130/G35562.1.
952 Hughen, K.A., Heaton, T.J., 2020. Updated Cariaco Basin ^{14}C Calibration Dataset from 0–60 cal
953 kyr BP. Radiocarbon 62, 1001–1043. https://doi.org/10.1017/RDC.2020.53.
954 Hughen, K.A., Southon, J.R., Lehman, S.J., Overpeck, J.T., 2000. Synchronous Radiocarbon and
955 Climate Shifts During the Last Deglaciation. Science 290, 1951.
956 https://doi.org/10.1126/science.290.5498.1951.
957 Hüls, M., Zahn, R., 2000. Millennial-scale sea surface temperature variability in the western
958 tropical North Atlantic from planktonic foraminiferal census counts. Paleoceanography 15,
959 659–678. https://doi.org/10.1029/1999PA000462.
960 Jaeschke, A., Rühlemann, C., Arz, H., Heil, G., Lohmann, G., 2007. Coupling of millennial-scale
961 changes in sea surface temperature and precipitation off northeastern Brazil with high-
962 latitude climate shifts during the last glacial period. Paleoceanography 22.
963 https://doi.org/10.1029/2006PA001391.
964 Johns, W.E., Lee, T.N., Beardsley, R.C., Candela, J., Limeburner, R., Castro, B., 1998. Annual
965 Cycle and Variability of the North Brazil Current. J. Phys. Oceanogr. 28, 103–128.
966 https://doi.org/10.1175/1520-0485(1998)028<0103:ACAVOT>2.0.CO;2.

967 Johns, W.E., Townsend, T.L., Fratantoni, D.M., Wilson, W.D., 2002. On the Atlantic inflow to
968 the Caribbean Sea. Deep Sea Res. Part I Oceanogr. Res. Pap. 49, 211–243.
969 https://doi.org/doi:10.1016/S0967-0637(01)00041-3.
970 Kageyama, M., Merkel, U., Otto-Bliesner, B., Prange, M., Abe-Ouchi, A., Lohmann, G., Ohgaito,
971 R., Roche, D.M., Singarayer, J., Swingedouw, D., Zhang, X., 2013. Climatic impacts of
972 fresh water hosing under Last Glacial Maximum conditions: a multi-model study. Clim.
973 Past. 9, 935–953. https://doi.org/10.5194/cp-9-935-2013.
974 Kanner, L.C., Burns, S.J., Cheng, H., Edwards, R.L., 2012. High-Latitude Forcing of the South
975 American Summer Monsoon During the Last Glacial. Science 335, 570.
976 https://doi.org/10.1126/science.1213397.
977 Kilbourne, K.H., Quinn, T.M., Guilderson, T.P., Webb, R.S., Taylor, F.W., 2007. Decadal- to
978 interannual-scale source water variations in the Caribbean Sea recorded by Puerto Rican
979 coral radiocarbon. Clim. Dyn. 29, 51–62. https://doi.org/10.1007/s00382-007-0224-2.
980 Kotov, S., Pälike, H., 2018. QAnalySeries – a cross-platform time series tuning and analysis tool.
981 AGU Fall meeting.
982 Labeyrie, L., 1999. CAMPAGNE INTERPOLE MD99-114/ IMAGES V , Gif/Yvette cedex
983 France, IPEV-Dept- Océanographique.
984 Labeyrie, L.D., Zahn, R., 2005a. Physical properties of sediment core MD99-2198.
985 https://doi.org/10.1594/PANGAEA.253083.
986 Labeyrie, L.D., Zahn, R., 2005b. Physical properties of sediment core MD99-2199.
987 https://doi.org/10.1594/PANGAEA.253084.
988 Lambelet, M., van de Flierdt, T., Crocket, K., Rehkämper, M., Kreissig, K., Coles, B., Rijkenberg,
989 M.J.A., Gerringa, L.J.A., de Baar, H.J.W., Steinfeldt, R., 2016. Neodymium isotopic

composition and concentration in the western North Atlantic Ocean: Results from the GEOTRACES GA02 section. Geochim. Cosmochim. Acta 177, 1–29. https://doi.org/10.1016/j.gca.2015.12.019.

Laskar, J., Robutel, P., Joutel, F., Gastineau, M., Correia, A.C.M., Levrard, B., 2004. A long-term numerical solution for the insolation quantities of the Earth. Astron. Astrophys. 428, 261–285. http://dx.doi.org/10.1051/0004-6361:20041335.

Lehner, B., Linke, S., Thieme, M., 2019. HydroATLAS version 1.0. figshare. Dataset. https://doi.org/10.6084/m9.figshare.9890531.v1.

Li, C., Born, A., 2019. Coupled atmosphere-ice-ocean dynamics in Dansgaard-Oeschger events. Quat. Sci. Rev., *203*, 1-20. https://doi.org/10.1016/j.quascirev.2018.10.031.

Liu, Z., Alexander, M., 2007. Atmospheric bridge, oceanic tunnel, and global climatic teleconnections. Rev. Geophys. 45. https://doi.org/10.1029/2005RG000172.

López, R., López, J.M., Morell, J., Corredor, J.E., Del Castillo, C.E., 2013. Influence of the Orinoco River on the primary production of eastern Caribbean surface waters. J Geophy Res: Oceans 118, 4617–4632. https://doi.org/10.1002/jgrc.20342.

López-Otálvaro, G.-E.L., Flores, J.A., Sierro, F.J., Cacho, I., Grimalt, J.-O., et. al., 2008. Late Pleistocene paleoproductivity patterns during the last climatic cycle in the Guyana Basin as revealed by calcareous nannoplankton. eEarth Discussions 11–40.

Lyle, M., Lyle, A.O., Gorgas, T., Holbourn, A., Westerhold, T., Hathorne, E., Katsunori, K., Yamamoto, S., 2012. Data report: raw and normalized elemental data along the Site U1338 splice from X-ray fluorescence scanning. In Pälike, H., Lyle, M., Nishi, H., Raffi, I., Gamage, K., Klaus, A., and the Expedition 320/321 Scientists, Proc. IODP, 320/321: Tokyo (Integrated Ocean Drilling Program Management International, Inc.).

1013 Lynch-Stieglitz, J., 2017. The Atlantic Meridional Overturning Circulation and Abrupt Climate
1014 Change. Annu. Rev. Mar. Sci. 9, 83–104. https://doi.org/10.1146/annurev-marine-010816-
1015 060415.
1016 Lynch-Stieglitz, J., Schmidt, M.W., Gene Henry, L., Curry, W.B., Skinner, L.C., Mulitza, S.,
1017 Zhang, R., Chang, P., 2014. Muted change in Atlantic overturning circulation over some
1018 glacial-aged Heinrich events. Nature Geosci 7, 144–150.
1019 https://doi.org/10.1038/ngeo2045.
1020 Marcott, S.A., Clark, P.U., Padman, L., Klinkhammer, G.P., Springer, S.R., Liu, Z., Otto-Bliesner,
1021 B.L., Carlson, A.E., Ungerer, A., Padman, J., He, F., Cheng, J., Schmittner, A., 2011. Ice-
1022 shelf collapse from subsurface warming as a trigger for Heinrich events. Proc. Natl. Acad.
1023 Sci .U.S.A. 108, 13415–13419. https://doi.org/10.1073/pnas.1104772108.
1024 Markle, B.R., Steig, E.J., Buizert, C., Schoenemann, S.W., Bitz, C.M., Fudge, T.J., Pedro, J.B.,
1025 Ding, Q., Jones, T.R., White, J.W.C., Sowers, T., 2017. Global atmospheric
1026 teleconnections during Dansgaard–Oeschger events. Nature Geosci. 10, 36–40.
1027 https://doi.org/10.1038/ngeo2848.
1028 Martinez, C., Goddard, L., Kushnir, Y., Ting, M., 2019. Seasonal climatology and dynamical
1029 mechanisms of rainfall in the Caribbean. Clim. Dyn. 53, 825–846.
1030 https://doi.org/10.1007/s00382-019-04616-4.
1031 Martinez, J.M., Guyot, J.L., Filizola, N., Sondag, F., 2009. Increase in suspended sediment
1032 discharge of the Amazon River assessed by monitoring network and satellite data. Catena
1033 79, 257–264. https://doi.org/10.1016/j.catena.2009.05.011.

1034 Maslin, M., Knutz, P.C., Ramsay, T., 2006. Millennial-scale sea-level control on avulsion events
1035 on the Amazon Fan. Quat. Sci Rev. 25, 3338–3345.
1036 https://doi.org/10.1016/j.quascirev.2006.10.012.
1037 McGee, D., Moreno-Chamarro, E., Green, B., Marshall, J., Galbraith, E., Bradtmiller, L., 2018.
1038 Hemispherically asymmetric trade wind changes as signatures of past ITCZ shifts. Quat.
1039 Sci Rev. 180, 214–228. https://doi.org/10.1016/j.quascirev.2017.11.020.
1040 Meade, R. H., 1994. Suspended sediments of the modern Amazon and Orinoco rivers. Quat. Int.,
1041 21, 29-39. https://doi.org/10.1016/1040-6182(94)90019-1.
1042 Meade, R.H., 2007. Transcontinental Moving and Storage: the Orinoco and Amazon Rivers
1043 Transfer the Andes to the Atlantic, in: Large Rivers. John Wiley & Sons, Ltd, pp. 45–63.
1044 https://doi.org/10.1002/9780470723722.ch4.
1045 Menviel, L.C., Skinner, L.C., Tarasov, L., Tzedakis, P.C., 2020. An ice–climate oscillatory
1046 framework for Dansgaard–Oeschger cycles. Nature Reviews Earth & Environment 1, 677–
1047 693. https://doi.org/10.1038/s43017-020-00106-y.
1048 Milliman, J.D., Butenko, J., Barbot, J.P., Hedberg, J., 1982. Depositional patterns of modern
1049 Orinoco/Amazon muds on the northern Venezuelan shelf. J Mar Res 40(3), 643–657.
1050 Mora, A., Moreau, C., Moquet, J. S., Gallay, M., Mahlknecht, J., Laraque, A., 2020. Hydrological
1051 control, fractionation, and fluxes of dissolved rare earth elements in the lower Orinoco
1052 River, Venezuela. Appl. Geochem. 112, 104462.
1053 https://doi.org/10.1016/j.apgeochem.2019.104462.
1054 Mosblech, N.A.S., Bush, M.B., Gosling, W.D., Hodell, D., Thomas, L., van Calsteren, P., Correa-
1055 Metrio, A., Valencia, B.G., Curtis, J., van Woesik, R., 2012. North Atlantic forcing of

1056 Amazonian precipitation during the last ice age. Nature Geosci 5, 817–820.
1057 https://doi.org/10.1038/ngeo1588.
1058 Muhs, D.R., Budahn, J.R., Prospero, J.M., Carey, S.N., 2007. Geochemical evidence for African
1059 dust inputs to soils of western Atlantic islands: Barbados, the Bahamas, and Florida. J
1060 Geophy Res F: Earth Surface 112. https://doi.org/10.1029/2005JF000445.
1061 Mulitza, S., Chiessi, C.M., Schefuß, E., Lippold, J., Wichmann, D., Antz, B., Mackensen, A., Paul,
1062 A., Prange, M., Rehfeld, K., Werner, M., Bickert, T., Frank, N., Kuhnert, H., Lynch-
1063 Stieglitz, J., Portilho-Ramos, R.C., Sawakuchi, A.O., Schulz, M., Schwenk, T., Tiedemann,
1064 R., Vahlenkamp, M., Zhang, Y., 2017. Synchronous and proportional deglacial changes in
1065 Atlantic meridional overturning and northeast Brazilian precipitation. Paleoceanography
1066 32, 622–633. https://doi.org/10.1002/2017PA003084.
1067 Nace, T.E., Baker, P.A., Dwyer, G.S., Silva, C.G., Rigsby, C.A., Burns, S.J., Giosan, L., Otto-
1068 Bliesner, B., Liu, Z., Zhu, J., 2014. The role of North Brazil Current transport in the
1069 paleoclimate of the Brazilian Nordeste margin and paleoceanography of the western
1070 tropical Atlantic during the late Quaternary. Palaeogeogr. Palaeoclimatol. Palaeoecol 415,
1071 3–13. https://doi.org/10.1016/j.palaeo.2014.05.030.
1072 NGRIP community members, 2004. High-resolution record of Northern Hemisphere climate
1073 extending into the last interglacial period. Nature 431, 147–151.
1074 https://doi.org/10.1038/nature02805.
1075 Nürnberg, D., Riff, T., Bahr, A., Karas, C., Meier, K., Lippold, J., 2021. Western boundary current
1076 in relation to Atlantic Subtropical Gyre dynamics during abrupt glacial climate
1077 fluctuations. Glob. Planet. Change 201, 103497.
1078 https://doi.org/10.1016/j.gloplacha.2021.103497.

1079 Pahnke, K., Goldstein, S.L., Hemming, S.R., 2008. Abrupt changes in Antarctic Intermediate
1080 Water circulation over the past 25,000 years. Nature Geosci 1, 870–874.
1081 https://doi.org/10.1038/ngeo360.
1082 Paillard, D., Labeyrie, L., Yiou, P., 1996. Macintosh program performs time-series analysis. Eos,
1083 Transactions American Geophysical Union 77, 379–379.
1084 https://doi.org/10.1029/96EO00259.
1085 Parker, A.O., Schmidt, M.W., Chang, P., 2015. Tropical North Atlantic subsurface warming events
1086 as a fingerprint for AMOC variability during Marine Isotope Stage 3. Paleoceanography
1087 30, 1425–1436. https://doi.org/10.1002/2015PA002832.
1088 Pedro, J.B., Jochum, M., Buizert, C., He, F., Barker, S., Rasmussen, S.O., 2018. Beyond the
1089 bipolar seesaw: Toward a process understanding of interhemispheric coupling. Quat Sci
1090 Rev 192, 27–46. https://doi.org/10.1016/j.quascirev.2018.05.005.
1091 Peterson, L.C., Haug, G.H., Hughen, K.A., Röhl, U., 2000. Rapid Changes in the Hydrologic Cycle
1092 of the Tropical Atlantic During the Last Glacial. Science 290, 1947.
1093 https://doi.org/10.1126/science.290.5498.1947.
1094 Phillips, S.C., Johnson, J.E., Giosan, L., Rose, K., 2014. Monsoon-influenced variation in
1095 productivity and lithogenic sediment flux since 110 ka in the offshore Mahanadi Basin,
1096 northern Bay of Bengal. Marine and Petroleum Geology 58, 502–525.
1097 https://doi.org/10.1016/j.marpetgeo.2014.05.007.
1098 Piacsek, P., Behling, H., Ballalai, J.M., Nogueira, J., Venancio, I.M., Albuquerque, A.L.S., 2021.
1099 Reconstruction of vegetation and low latitude ocean-atmosphere dynamics of the past 130
1100 kyr, based on South American montane pollen types. Glob. Planet. Change 201, 103477.
1101 https://doi.org/10.1016/j.gloplacha.2021.103477.

1102 Picard, M., Schneider, J.-L., Boudon, G., 2006. Contrasting sedimentary processes along a
1103 convergent margin: the Lesser Antilles arc system. Geo-Marine Letters 26, 397.
1104 https://doi.org/10.1007/s00367-006-0046-y.
1105 Poveda, G., Waylen, P.R., Pulwarty, R.S., 2006. Annual and inter-annual variability of the present
1106 climate in northern South America and southern Mesoamerica. Palaeogeogr.
1107 Palaeoclimatol. Palaeoecol 234, 3–27. https://doi.org/10.1016/j.palaeo.2005.10.031.
1108 QGIS Development Team (2020). QGIS Geographic Information System. Open Source
1109 Geospatial Foundation Project. http://qgis.osgeo.org.
1110 Rama-Corredor, O., Martrat, B., Grimalt, J.O., López-Otálvaro, G.E., Flores, J.A., Sierro, F., 2015.
1111 Parallelisms between sea surface temperature changes in the western tropical Atlantic
1112 (Guiana Basin) and high latitude climate signals over the last 140 000 years. Clim. Past 11,
1113 1297–1311. https://doi.org/10.5194/cp-11-1297-2015.
1114 Rasmussen, S.O., Bigler, M., Blockley, S.P., Blunier, T., Buchardt, S.L., Clausen, H.B.,
1115 Cvijanovic, I., Dahl-Jensen, D., Johnsen, S.J., Fischer, H., Gkinis, V., Guillevic, M., Hoek,
1116 W.Z., Lowe, J.J., Pedro, J.B., Popp, T., Seierstad, I.K., Steffensen, J.P., Svensson, A.M.,
1117 Vallelonga, P., Vinther, B.M., Walker, M.J.C., Wheatley, J.J., Winstrup, M., 2014. A
1118 stratigraphic framework for abrupt climatic changes during the Last Glacial period based
1119 on three synchronized Greenland ice-core records: refining and extending the INTIMATE
1120 event stratigraphy. Quat Sci Rev 106, 14–28.
1121 https://doi.org/10.1016/j.quascirev.2014.09.007.
1122 Rasmussen, T.L., Thomsen, E., Moros, M., 2016. North Atlantic warming during Dansgaard-
1123 Oeschger events synchronous with Antarctic warming and out-of-phase with Greenland
1124 climate. Sci. Rep. 6, 20535. https://doi.org/10.1038/srep20535.

1125 Reid, P.R., Carey, S.N., Ross, D.R., 1996. Late Quaternary sedimentation in the Lesser Antilles
1126 island arc. GSA Bulletin 108, 78–100. https://doi.org/10.1130/0016-
1127 7606(1996)108<0078:LQSITL>2.3.CO;2.
1128 Reimer, P.J., Bard, E., Bayliss, A., Beck, J.W., Blackwell, P.G., Ramsey, C.B., Buck, C.E., Cheng,
1129 H., Edwards, R.L., Friedrich, M., Grootes, P.M., Guilderson, T.P., Haflidason, H., Hajdas,
1130 I., Hatté, C., Heaton, T.J., Hoffmann, D.L., Hogg, A.G., Hughen, K.A., Kaiser, K.F.,
1131 Kromer, B., Manning, S.W., Niu, M., Reimer, R.W., Richards, D.A., Scott, E.M., Southon,
1132 J.R., Staff, R.A., Turney, C.S.M., van der Plicht, J., 2013. IntCal13 and Marine13
1133 Radiocarbon Age Calibration Curves 0–50,000 Years cal BP. Radiocarbon 55, 1869–1887.
1134 https://doi.org/10.2458/azu_js_rc.55.16947.
1135 Reißig, S., Nürnberg, D., Bahr, A., Poggemann, D.-W., Hoffmann, J., 2019. Southward
1136 Displacement of the North Atlantic Subtropical Gyre Circulation System During North
1137 Atlantic Cold Spells. Paleoceanography and Paleoclimatology 34, 866–885.
1138 https://doi.org/10.1029/2018PA003376.
1139 Richter, T.O., van der Gaast, S., Koster, B., Vaars, A., Gieles, R., de Stigter, H.C., De Haas, H.,
1140 van Weering, T.C.E., 2006. The Avaatech XRF Core Scanner: technical description and
1141 applications to NE Atlantic sediments. Geol. Soc. London, Special Publications 267, 39.
1142 https://doi.org/10.1144/GSL.SP.2006.267.01.03.
1143 Roberts, W.H.G., Hopcroft, P.O., 2020. Controls on the Tropical Response to Abrupt Climate
1144 Changes. Geophys. Res. Lett. 47, e2020GL087518.
1145 https://doi.org/10.1029/2020GL087518.

1146 Rodrigues, R.R., Rothstein, L.M., Wimbush, M., 2007. Seasonal Variability of the South
1147 Equatorial Current Bifurcation in the Atlantic Ocean: A Numerical Study. J. Phys.
1148 Oceanogr. 37, 16–30. https://doi.org/10.1175/JPO2983.1
1149 Rousseau, T. C., Roddaz, M., Moquet, J. S., Delgado, H. H., Calves, G., Bayon, G., 2019. Controls
1150 on the geochemistry of suspended sediments from large tropical South American rivers
1151 (Amazon, Orinoco and Maroni). Chem. Geol. 522, 38-54.
1152 https://doi.org/10.1016/j.chemgeo.2019.05.027.
1153 Roy, P.D., Quiroz-Jiménez, J.D., Pérez-Cruz, L.L., Lozano-García, S., Metcalfe, S.E., Lozano-
1154 Santacruz, R., López-Balbiaux, N., Sánchez-Zavala, J.L., Romero, F.M., 2013. Late
1155 Quaternary paleohydrological conditions in the drylands of northern Mexico: a summer
1156 precipitation proxy record of the last 80 cal ka BP. Quat. Sci Rev. 78, 342–354.
1157 https://doi.org/10.1016/j.quascirev.2012.11.020.
1158 Rühlemann, C., Diekmann, B., Mulitza, S., Frank, M., 2001. Late Quaternary changes of western
1159 equatorial Atlantic surface circulation and Amazon lowland climate recorded in Ceará Rise
1160 deep-sea sediments. Paleoceanography 16, 293–305.
1161 https://doi.org/10.1029/1999PA000474.
1162 Rühlemann, C., Mulitza, S., Müller, P.J., Wefer, G., Zahn, R., 1999. Warming of the tropical
1163 Atlantic Ocean and slowdown of thermohaline circulation during the last deglaciation.
1164 Nature 402, 511–514. https://doi.org/doi:10.1038/990069.
1165 Schlitzer, R., 2017. Ocean Data View, software available at: http://odv.awi.de, last access:
1166 November 2017.
1167 Schlünz, B., Schneider, R., Müller, P., Wefer, G., 2000. Late Quaternary organic carbon
1168 accumulation south of Barbados: influence of the Orinoco and Amazon rivers? Deep-Sea

1169 Res. Part I: Oceanog. Res. 47, 1101–1124. https://doi.org/10.1016/S0967-0637(99)00076-
1170 X.
1171 Schlünz, B., Schneider, R.R., Müller, P.J., Showers, W.J., Wefer, G., 1999. Terrestrial organic
1172 carbon accumulation on the Amazon deep sea fan during the last glacial sea level low stand.
1173 Chem. Geol. 159, 263–281. https://doi.org/10.1016/S0009-2541(99)00041-8.
1174 Schmidt, M.W., Chang, P., Hertzberg, J.E., Them, T.R., J, L., Otto-Bliesner, B.L., 2012. Impact
1175 of abrupt deglacial climate change on tropical Atlantic subsurface temperatures. Proc. Natl.
1176 Acad. Sci .U.S.A. https://doi.org/10.1073/pnas.1207806109.
1177 Schmidt, M.W., Lynch-Stieglitz, J., 2011. Florida Straits deglacial temperature and salinity
1178 change: Implications for tropical hydrologic cycle variability during the Younger Dryas.
1179 Paleoceanography 26. https://doi.org/10.1029/2011PA002157.
1180 Schmidt, M.W., Vautravers, M.J., Spero, H.J., 2006. Rapid subtropical North Atlantic salinity
1181 oscillations across Dansgaard–Oeschger cycles. Nature 443, 561–564.
1182 https://doi.org/doi:10.1038/nature05121.
1183 Schneider, T., Bischoff, T., Haug, G.H., 2014. Migrations and dynamics of the intertropical
1184 convergence zone. Nature 513, 45–53. https://doi.org/10.1038/nature13636.
1185 Schott, F.A., Fischer, J., Stramma, L., 1998. Transports and Pathways of the Upper-Layer
1186 Circulation in the Western Tropical Atlantic. J Phys Ocean 28, 1904–1928.
1187 https://doi.org/10.1175/1520-0485(1998)028<1904:TAPOTU>2.0.CO;2.
1188 Sessford, E.G., Jensen, M.F., Tisserand, A.A., Muschitiello, F., Dokken, T., Nisancioglu, K.H.,
1189 Jansen, E., 2019. Consistent fluctuations in intermediate water temperature off the coast of
1190 Greenland and Norway during Dansgaard-Oeschger events. Quat Sci Rev 223, 105887.
1191 https://doi.org/10.1016/j.quascirev.2019.105887.

1192 Shankar, R., Prabhu, C.N., Warrier, A.K., Kumara, G.V., Sekar, B., 2006. A Multi-decadal Rock
1193 Magnetic Record of Monsoonal Variations During the Past 3,700 Years from a Tropical
1194 Indian Tank. J Geol Soc India 68, 447–459.
1195 Silva, V.B.S., Kousky, V.E., 2012. The South American monsoon system, climatology and
1196 variability. In: Wang, S.-Y. (Ed.), Modern Climatology. In Tech China, pp. 123-152.
1197 Spratt, R.M., Lisiecki, L.E., 2016. A Late Pleistocene sea level stack. Clim. Past 12, 1079–1092.
1198 https://doi.org/10.5194/cp-12-1079-2016.
1199 Stocker, T.F., Johnsen, S.J., 2003. A minimum thermodynamic model for the bipolar seesaw.
1200 Paleoceanography 18. https://doi.org/10.1029/2003PA000920
1201 Stramma, L., Schott, F., 1999. The mean flow field of the tropical Atlantic Ocean. Deep Sea
1202 Research Part II: Topical Studies in Oceanography 46, 279–303.
1203 https://doi.org/10.1016/S0967-0645(98)00109-X
1204 Stríkis, N.M., Cruz, F.W., Barreto, E.A.S., Naughton, F., Vuille, M., Cheng, H., Voelker, A.H.L.,
1205 Zhang, H., Karmann, I., Edwards, R.L., Auler, A.S., Santos, R.V., Sales, H.R., 2018. South
1206 American monsoon response to iceberg discharge in the North Atlantic. Proc Natl Acad
1207 Sci USA 115, 3788. https://doi.org/10.1073/pnas.1717784115.
1208 Ternan, J.L., Williams, A.G., Francis, C., 1989. Land Capability Classification in Grenada, West
1209 Indies. Mountain Research and Development 9, 71–82. https://doi.org/10.2307/3673466.
1210 Them, T.R., Schmidt, M.W., Lynch-Stieglitz, J., 2015. Millennial-scale tropical atmospheric and
1211 Atlantic Ocean circulation change from the Last Glacial Maximum and Marine Isotope
1212 Stage 3. Earth Planet. Sci. Lett 427, 47–56. https://doi.org/10.1016/j.epsl.2015.06.062.

1213 Thornalley, D.J.R., Barker, S., Becker, J., Hall, I.R., Knorr, G., 2013. Abrupt changes in deep
1214 Atlantic circulation during the transition to full glacial conditions. Paleoceanography 28,
1215 253–262. https://doi.org/10.1002/palo.20025.
1216 Timmermann, A., Krebs, U., Justino, F., Goosse, H., Ivanochko, T., 2005. Mechanisms for
1217 millennial-scale global synchronization during the last glacial period. Paleoceanography
1218 20. https://doi.org/10.1029/2004PA001090.
1219 Tjallingii, R., Röhl, U., Kölling, M., Bickert, T., 2007. Influence of the water content on X-ray
1220 fluorescence core-scanning measurements in soft marine sediments. Geochem. Geophys.
1221 Geosyst. 8, Q02004. https://doi.org/10.1029/2006GC001393.
1222 Vanderaveroet, P., Averbuch, O., Deconinck, J., Chamley, H., 1999. A record of
1223 glacial/interglacial alternations in Pleistocene sediments off New Jersey expressed by clay
1224 mineral, grain-size and magnetic susceptibility data. Mar Geology 159, 79–92.
1225 Venancio, I.M., Mulitza, S., Govin, A., Santos, T.P., Lessa, D.O., Albuquerque, A.L.S., Chiessi,
1226 C.M., Tiedemann, R., Vahlenkamp, M., Bickert, T., Schulz, M., 2018. Millennial- to
1227 Orbital-Scale Responses of Western Equatorial Atlantic Thermocline Depth to Changes in
1228 the Trade Wind System Since the Last Interglacial. Paleoceanography and
1229 Paleoclimatology 33, 1490–1507. https://doi.org/10.1029/2018PA003437.
1230 Vink, A., Rühlemann, C., Zonneveld, K.A.F., Mulitza, S., Hüls, M., Willems, H., 2001. Shifts in
1231 the position of the north equatorial current and rapid productivity changes in the western
1232 tropical Atlantic during the last glacial. Paleoceanography 16, 479–490.
1233 https://doi.org/10.1029/2000PA000582.
1234 Vuille, M., Burns, S.J., Taylor, B.E., Cruz, F.W., Bird, B.W., Abbott, M.B., Kanner, L.C., Cheng,
1235 H., Novello, V.F., 2012. A review of the South American monsoon history as recorded in

1236 stable isotopic proxies over the past two millennia. Clim. Past 8, 1309-1321.
1237 https://doi.org/10.5194/cp-8-1309-2012.
1238 Waelbroeck, C., Lougheed, B.C., Vazquez Riveiros, N., Missiaen, L., Pedro, J., Dokken, T.,
1239 Hajdas, I., Wacker, L., Abbott, P., Dumoulin, J.-P., Thil, F., Eynaud, F., Rossignol, L.,
1240 Fersi, W., Albuquerque, A.L., Arz, H., Austin, W.E.N., Came, R., Carlson, A.E., Collins,
1241 J.A., Dennielou, B., Desprat, S., Dickson, A., Elliot, M., Farmer, C., Giraudeau, J.,
1242 Gottschalk, J., Henderiks, J., Hughen, K., Jung, S., Knutz, P., Lebreiro, S., Lund, D.C.,
1243 Lynch-Stieglitz, J., Malaizé, B., Marchitto, T., Martínez-Méndez, G., Mollenhauer, G.,
1244 Naughton, F., Nave, S., Nürnberg, D., Oppo, D., Peck, V., Peeters, F.J.C., Penaud, A.,
1245 Portilho-Ramos, R. da C., Repschläger, J., Roberts, J., Rühlemann, C., Salgueiro, E.,
1246 Sanchez Goni, M.F., Schönfeld, J., Scussolini, P., Skinner, L.C., Skonieczny, C.,
1247 Thornalley, D., Toucanne, S., Rooij, D.V., Vidal, L., Voelker, A.H.L., Wary, M., Weldeab,
1248 S., Ziegler, M., 2019. Consistently dated Atlantic sediment cores over the last 40 thousand
1249 years. Sci Data 6, 165. https://doi.org/10.1038/s41597-019-0173-8.
1250 WAIS Divide Project Members.,Buizert, C., Adrian, B., Ahn, J., Albert, M., Alley, R.B.,
1251 Baggenstos, D., Bauska, T.K., Bay, R.C., Bencivengo, B.B., Bentley, C.R., Brook, E.J.,
1252 Chellman, N.J., Clow, G.D., Cole-Dai, J., Conway, H., Cravens, E., Cuffey, K.M., Dunbar,
1253 N.W., Edwards, J.S., Fegyveresi, J.M., Ferris, D.G., Fitzpatrick, J.J., Fudge, T.J., Gibson,
1254 C.J., Gkinis, V., Goetz, J.J., Gregory, S., Hargreaves, G.M., Iverson, N., Johnson, J.A.,
1255 Jones, T.R., Kalk, M.L., Kippenhan, M.J., Koffman, B.G., Kreutz, K., Kuhl, T.W., Lebar,
1256 D.A., Lee, J.E., Marcott, S.A., Markle, B.R., Maselli, O.J., McConnell, J.R., McGwire,
1257 K.C., Mitchell, L.E., Mortensen, N.B., Neff, P.D., Nishiizumi, K., Nunn, R.M., Orsi, A.J.,
1258 Pasteris, D.R., Pedro, J.B., Pettit, E.C., Buford Price, P., Priscu, J.C., Rhodes, R.H., Rosen,

1259 J.L., Schauer, A.J., Schoenemann, S.W., Sendelbach, P.J., Severinghaus, J.P., Shturmakov,
1260 A.J., Sigl, M., Slawny, K.R., Souney, J.M., Sowers, T.A., Spencer, M.K., Steig, E.J.,
1261 Taylor, K.C., Twickler, M.S., Vaughn, B.H., Voigt, D.E., Waddington, E.D., Welten, K.C.,
1262 Wendricks, A.W., White, J.W.C., Winstrup, M., Wong, G.J., Woodruff, T.E., WAIS
1263 Divide Project Members, 2015. Precise interpolar phasing of abrupt climate change during
1264 the last ice age. Nature 520, 661–665. https://doi.org/10.1038/nature14401.
1265 Wan, X., Chang, P., Saravanan, R., Zhang, R., Schmidt, M.W., 2009. On the interpretation of
1266 Caribbean paleo-temperature reconstructions during the Younger Dryas. Geophys. Res.
1267 Lett. 36. https://doi.org/10.1029/2008GL035805.
1268 Wang, X., Auler, A.S., Edwards, R.L., Cheng, H., Ito, E., Wang, Y., Kong, X., Solheid, M., 2007.
1269 Millennial-scale precipitation changes in southern Brazil over the past 90,000 years.
1270 Geophys. Res. Lett. 34. https://doi.org/10.1029/2007GL031149.
1271 Warken, S.F., Scholz, D., Spötl, C., Jochum, K.P., Pajón, J.M., Bahr, A., Mangini, A., 2019.
1272 Caribbean hydroclimate and vegetation history across the last glacial period. Quat. Sci Rev.
1273 218, 75–90. https://doi.org/10.1016/j.quascirev.2019.06.019.
1274 Warken, S.F., Vieten, R., Winter, A., Spötl, C., Miller, T.E., Jochum, K.P., Schröder-Ritzrau, A.,
1275 Mangini, A., Scholz, D., 2020. Persistent Link Between Caribbean Precipitation and
1276 Atlantic Ocean Circulation During the Last Glacial Revealed by a Speleothem Record
1277 From Puerto Rico. Paleoceanography and Paleoclimatology 35, e2020PA003944.
1278 https://doi.org/10.1029/2020PA003944.
1279 Warne, A.G., Meade, R.H., White, W.A., Guevara, E.H., Gibeaut, J., Smyth, R.C., Aslan, A.,
1280 Tremblay, T., 2002. Regional controls on geomorphology, hydrology, and ecosystem

1281 integrity in the Orinoco Delta, Venezuela. Geomorphology 44, 273–307.
1282 https://doi.org/10.1016/S0169-555X(01)00179-9.
1283 Weldeab, S., Schneider, R.R., Kölling, M., 2006. Deglacial sea surface temperature and salinity
1284 increase in the western tropical Atlantic in synchrony with high latitude climate
1285 instabilities. Earth Planet. Sci. Lett. 241, 699–706.
1286 https://doi.org/10.1016/j.epsl.2005.11.012.
1287 Weltje, G.J., Tjallingii, R., 2008. Calibration of XRF core scanners for quantitative geochemical
1288 logging of sediment cores: Theory and application. Earth Planet. Sci. Lett 274, 423–438.
1289 https://doi.org/10.1016/j.epsl.2008.07.054.
1290 Wilson, K.E., Maslin, M.A., Burns, S.J., 2011. Evidence for a prolonged retroflection of the North
1291 Brazil Current during glacial stages. Palaeogeogr. Palaeoclimatol. Palaeoecol. 301, 86–96.
1292 https://doi.org/10.1016/j.palaeo.2011.01.003.
1293 Wu, L., Wilson, D.J., Wang, R., Yin, X., Chen, Z., Xiao, W., Huang, M., 2020. Evaluating Zr/Rb
1294 Ratio From XRF Scanning as an Indicator of Grain-Size Variations of Glaciomarine
1295 Sediments in the Southern Ocean. Geochem. Geophys. Geosyst. 21, e2020GC009350.
1296 https://doi.org/10.1029/2020GC009350.
1297 Zarriess, M., Johnstone, H., Prange, M., Steph, S., Groeneveld, J., Mulitza, S., Mackensen, A.,
1298 2011. Bipolar seesaw in the northeastern tropical Atlantic during Heinrich stadials.
1299 Geophys. Res. Lett. 38. https://doi.org/10.1029/2010GL046070.
1300 Zhang, D., Msadek, R., McPhaden, M.J., Delworth, T., 2011. Multidecadal variability of the North
1301 Brazil Current and its connection to the Atlantic meridional overturning circulation. J.
1302 Geophys. Res.: Oceans 116. https://doi.org/10.1029/2010JC006812.

1303 Zhang, X., Prange, M., Merkel, U., Schulz, M., 2015a. Spatial fingerprint and magnitude of
1304 changes in the Atlantic meridional overturning circulation during marine isotope stage 3.
1305 Geophys. Res. Lett. 42, 1903–1911. https://doi.org/10.1002/2014GL063003.
1306 Zhang, Y., Chiessi, C.M., Mulitza, S., Sawakuchi, A.O., Häggi, C., Zabel, M., Portilho-Ramos,
1307 R.C., Schefuß, E., Crivellari, S., Wefer, G., 2017. Different precipitation patterns across
1308 tropical South America during Heinrich and Dansgaard-Oeschger stadials. Quat. Sci Rev.
1309 177, 1–9. https://doi.org/10.1016/j.quascirev.2017.10.012.
1310 Zhang, Y., Chiessi, C.M., Mulitza, S., Zabel, M., Trindade, R.I.F., Hollanda, M.H.B.M., Dantas,
1311 E.L., Govin, A., Tiedemann, R., Wefer, G., 2015b. Origin of increased terrigenous supply
1312 to the NE South American continental margin during Heinrich Stadial 1 and the Younger
1313 Dryas. Earth Planet. Sci. Lett 432, 493–500. https://doi.org/10.1016/j.epsl.2015.09.054.
1314